

AD-A119 836

PRINCETON UNIV NJ DEPT OF CHEMICAL ENGINEERING

F/G 11/9

TORSIONAL BRAID ANALYSIS (TBA): TIME-TEMPERATURE-TRANSFORMATION--ETC(U)

SEP 82 J B ENNS, J K GILLHAM

N00014-76-C-0200

UNCLASSIFIED

TR-25

NL

1 of 1
AD A
1-9836

END
DATE
FORMED
11-82
DTIC

12

AD A119836

OFFICE OF NAVAL RESEARCH
Contract N00014-76-C-0200
Task No. NR 356-504
TECHNICAL REPORT NO.- 25

TORSIONAL BRAID ANALYSIS (TBA):
TIME-TEMPERATURE-TRANSFORMATION (TTT)
CURE DIAGRAMS OF THERMOSETTING EPOXY/AMINE SYSTEMS

by

John B. Enns and John K. Gillham

for publication in
"Instrumental and Physical Characterization of Macromolecules",
in Advances in Chemistry Series, American Chemical Society

PRINCETON UNIVERSITY
Polymer Materials Program
Department of Chemical Engineering
Princeton, New Jersey 08544

September 1982

DTIC
SELECTED
S OCT 4 1982 D
H

*Reproduction in whole or in part is permitted for
any purpose of the United States Government*

*This document has been approved for public release and sale;
its distribution is unlimited*

Principal Investigator
John K. Gillham
609/452-4694

DTIC COPY

20.

method for generating macroscopic TTT cure diagrams. The influence of chemical structure on the kinetics and macroscopic properties was investigated by comparing aliphatic and aromatic tetrafunctional amines with diepoxides of varying molecular weights. The paper also describes automation of the TBA instrument using a desk-top calculator.

Accession For	
NTIS GRA&I	<input checked="" type="checkbox"/>
DTIC TAB	<input type="checkbox"/>
Unannounced	<input type="checkbox"/>
Justification	<input type="checkbox"/>
By _____	
Distribution/	
Availability Codes	
Dist	Avail and/or Special
A	

DTIC
COPY
INSPECTED

TORSIONAL BRAID ANALYSIS (TBA):
TIME-TEMPERATURE-TRANSFORMATION (TTT)
CURE DIAGRAMS OF THERMOSETTING EPOXY/AMINE SYSTEMS

John B. Enns and John K. Gillham

*Polymer Materials Program
Department of Chemical Engineering
Princeton University
Princeton, NJ 08544*

ABSTRACT

The conversion of liquid resin to solid thermoset during the process of cure can be monitored using a substrate coated with the reactive system as the specimen in a torsion pendulum experiment (TBA). Measurement of times to gelation and vitrification at a series of temperatures results in an isothermal time-temperature-transformation (TTT) cure diagram which can be used for comparing different systems. In this report molecular and macroscopic TTT cure diagrams are considered: it is demonstrated that TBA is a convenient method for generating macroscopic TTT cure diagrams. The influence of chemical structure on the kinetics and macroscopic properties was investigated by comparing aliphatic and aromatic tetrafunctional amines with diepoxides of varying molecular weights. The paper also describes automation of the TBA instrument using a desk-top calculator.

INTRODUCTION

The torsion pendulum has proven to be an important and versatile tool in the study of dynamic mechanical properties of materials. In our laboratory it has been applied primarily to polymers, although elsewhere it has been applied to a wide variety of materials, ranging from liquids to metals and ceramics. The basis of its wide appeal lies in its fundamental simplicity: information about the complex modulus of the material under investigation is obtained by simply observing the decaying oscillations of the pendulum. After the pendulum is set in motion, it is permitted to oscillate freely at its resonant frequency while the amplitude of the oscillatory wave decays. In an unautomated system it is a relatively simple but tedious task to calculate the shear modulus (or rigidity) and the loss modulus from the period of the oscillation, its logarithmic decrement and the geometric constants of the system. The independent variable in the investigation of dynamic mechanical properties of a material is often temperature, but it can also be time, as in the case of chemically reactive or physically aging systems.

The technique is made more versatile by using a supported specimen as in Torsional Braid Analysis (TBA). Impregnating a glass braid with a solution (or melt) facilitates fabrication of a mounted specimen, permits use of small quantities of sample (25 mg), and permits study of the specimen in its solid and liquid states, as well as its change in state from liquid to solid and vice versa.

In this paper an automated Torsion Braid Analysis technique (1,2,3), controlled by a digital desktop computer, is discussed, and its utility in

the characterization of thermosetting resins is illustrated (4).

INSTRUMENTATION

A schematic diagram of the present torsion pendulum is shown in Figure 1. The pendulum is intermittently set into motion to generate a series of damped oscillations while the material behavior of the specimen changes with temperature and/or time. The non-driven, free oscillations are initiated by the step-displacement of an upper gear. The natural frequency range of the vibrations is 0.05 to 5 Hz. Conversion of the damped oscillations to electrical analog signals is accomplished using an optical transducer.

A key factor in the instrumentation was the development of a non-drag, optical transducer which produces an electrical response which is a linear function of the angular deformation of the pendulum. A polarizing disc is currently employed as the inertial member of the pendulum and a stationary second polarizer is positioned in front of a photocell whose response is a linear function of intensity. The intensity of light transmission through two polarizers is a cosine squared function of their angular displacement. Over a useful range symmetrical between the crossed and parallel positions of the pair of polarizers, the transmission function approaches linearity. As the properties of the specimen change, twisting of the specimen may cause the transducer to drift out of the linear range. The automated system was designed to compensate for this.

The specimen is supported in the cylindrical vertical shaft in a copper block around which are band heaters and cooling coils (for liquid nitrogen). The apparatus operates over a temperature range of -190°C to

400°C with a temperature spread of $< 1^\circ\text{C}$ over a 2-inch specimen. A temperature programmer/controller system permits experiments to be performed with linearly increasing, linearly decreasing, and isothermal ($\pm 0.1^\circ\text{C}$) temperature modes. Measurements have been made from 4°K and to 700°C in other apparatuses. The atmosphere is tightly controlled: inert, water-doped and reactive gases, and vacuum have been used. There are no electronic devices within the specimen chamber. Dry helium, rather than nitrogen, is used as an inert atmosphere because of its higher thermal conductivity at low temperatures. An on-line electronic hygrometer continuously monitors the water vapor content of atmospheres from < 20 to 20,000 parts per million H_2O .

The substrate which is generally used in a TBA experiment is a loose heat-cleaned glass braid containing about 3600 filaments (Figure 2). The large surface area of the assembly of filaments permits pickup of relatively large amounts of fluid and minimizes flow due to gravity. The contribution of the substrate to torsional properties of the composite specimen is minimized by using multifilaments (rather than a rod). A braid is employed in an attempt to balance twists in the component yarns. Solvent is removed from the solution-impregnated braid *in-situ* by heating above the boiling point of the solvent and into the fluid state of the polymer (compatible with thermal stability). The apparatus can also accommodate homogeneous specimens for conventional quantitative torsion pendulum studies [as in ASTM D-2236 (5)].

Substrates other than glass braids have been used; these include glass, carbon, cellulose and aramid fibers, metal foil (copper and aluminum), paper, single glass filament (as in fiber optics), metal wire, and plastic film (polyimide).

Material has been deposited on the substrate from solution, melt, emulsion and suspension (aqueous and non-aqueous), and from powder (by heating the substrate with an air-gun).

Two dynamic mechanical properties of the specimen, rigidity and damping, are obtained from the frequency and decay constants which characterize each wave. The TBA experiment provides plots of relative rigidity ($1/P^2$, where P is the period in seconds) and logarithmic decrement [$\Delta = \ln(\theta_i/\theta_{i+1})$, where θ_i is the amplitude of the i^{th} oscillation of a freely damped wave]. The relative rigidity is directly proportional to the in-phase or elastic portion of the shear modulus (G'); for example, for rod specimens of radius r and length L and for an oscillating system with moment of inertia I , $G' \cong (1/P^2)(8\pi IL/r^4)$. The logarithmic decrement is directly proportional to the ratio of the out-of-phase or viscous portion of the shear modulus (G'') to G' ($\Delta \cong \pi G''/G' = \pi \tan \delta$ where δ is the phase angle between the stress and strain). G' and G'' are material parameters of the specimen which characterize the storage and loss of mechanical energy on cyclic deformation, respectively. The energy stored during each cyclic deformation is $\frac{1}{2} G' \epsilon^2$ at strain ϵ and $\pi G'' \epsilon_{\text{max}}^2$ is an approximation for the energy dissipated per cycle, where ϵ_{max} is the peak strain.

A photograph of a pendulum/computer system which has been used since 1979 is shown in Figure 2. It shows the pendulum (enclosed in a cabinet, top left; cabinet door open, bottom left) and the major components of the assembly. The temperature controller, digital voltmeter, scanner, and computer are in the rack at the right. The printer is to the left of the rack, the plotter is to its right. The analog temperature and wave signals are continuously monitored on a two-pen strip-chart recorder. An atmosphere

control panel and liquid nitrogen container are shown in the background.

Film and impregnated braid specimens are shown at the bottom right of Figure 2. A film is shown assembled with upper and lower extension rods ready for lowering into the apparatus and then coupling with the polarizer disc of the transducer (shown bottom right). The polarizer disc contains a magnet at its center which couples to the end of the lower extension rod. Dimensions of specimens are selected so as to provide periods of oscillation in the range 0.2 to 20 s.

The system schematic for interfacing the TBA unit to a desktop computer which can synchronize the control and data processing of the torsion pendulum to produce results in real time is shown in Figure 3. Earlier experience (6) with a hierarchical digital computer system aided the development of the presently used data processing schemes (7).

For each damped wave the computer goes through a control sequence, which is schematically represented in Figure 4. An alignment motor rotates the pendulum (or the "stationary" polarizer) to the same reference position at the start of each control sequence. To initiate the oscillations, a second motor then rotates the pendulum a specified angular displacement against the tension of a spring. The pendulum is held in this cocked position until any oscillations set up by the alignment and cocking have subsided, at which time the clutch of the second motor is disengaged and the inertial mass swings back so as to oscillate about the reference position. The temperature (or time, for isothermal experiments) is then measured and the oscillation data are collected and processed. After plotting the reduced data, the oscillation is monitored until it decays to within specified limits and then the control cycle repeats.

The response function of the torsion pendulum to mechanical excitation is described to good approximation by

$$\theta(t) = \theta_0 \exp(-\alpha t) \cos(\omega t + \phi)$$

which is a solution to the equation of motion with form

$$\frac{d^2\theta}{dt^2} + A_1 \frac{d\theta}{dt} + A_2\theta = 0$$

where ω is the angular frequency, ϕ is a phase angle depending on timing of data acquisition, and θ_0 , $A_1 (= 2\alpha)$ and $A_2 (= \alpha^2 + \omega^2)$ are constants where α is the exponential decay constant. In complex format, the equation of motion is

$$I \frac{d^2\theta}{dt^2} + C(G' + iG'')\theta = 0$$

where G' and G'' are the in-phase and out-of-phase shear moduli, respectively, and C is a geometric constant.

Since an experiment may run over the course of several days and generate more than 1000 damped waves, manual techniques for reducing the experimental analog waves are slow and tedious. These have traditionally involved measuring the decay of successive peak amplitudes to provide the logarithmic decrement and the period $P (= 2\pi/\omega)$ for each wave. The data for torsion pendulum studies usually are presented as G' and Δ , G' and G'' ($\cong G'\Delta/\pi$) or as G' and $\tan\delta (= G''/G')$. For TBA experiments, due to the small size and the dependence of G' on the inverse fourth power of the

radius, the irregular geometry, and composite nature of the specimens, simplified parameters have been used. These parameters, which refer to the composite specimen, are relative rigidity ($1/P^2$) and the logarithmic decrement (Δ).

TIME-TEMPERATURE-TRANSFORMATION (TTT) CURE DIAGRAMS

The cure of thermosetting systems can be considered on a molecular as well as a macroscopic level. On the macroscopic Time-Temperature-Transformation (TTT) cure diagram (Figure 5) the cure can be characterized by the resin's rheology as a function of time and isothermal temperature. The boundaries between the regions delineated in Figure 5 are not as sharp as indicated, but rather diffuse; the time/temperature at which a transition occurs depends on the frequency of the test method and the dynamic mechanical property used to monitor it. ("Transition" is used in this paper to denote a change from one state to another.) Between T_{gel} and $T_{g\infty}$ the viscous liquid changes to a viscoelastic fluid, then to a rubber and finally to a glass. The "S"-shaped curve indicates the onset of vitrification which represents the time at which the glass transition temperature of the reacting system has reached the isothermal temperature of cure. $T_{g\infty}$ is the glass transition temperature of the fully cured resin, above which the system is a rubber in its fully cured state. As indicated in Figure 5 the time to vitrification passes through a minimum between T_{gel} and $T_{g\infty}$. This behavior reflects the competition between the increased rate constant for reaction and the increasing chemical conversion required to achieve vitrification as the temperature is increased. Also, as indicated in Figure 5, the time to vitrification passes through a maximum

between $T_{g, \text{resin}}$ and $T_{g, \text{gel}}$. This latter behavior reflects the competition between the temperature and time-dependences of viscosity of the reacting system. A liquid-to-rubber transition curve indicates the onset of the rubbery plateau. At lower isothermal temperatures (approaching $T_{g, \text{resin}}$) the state of the resin changes directly from a liquid to a glass without going through an intermediate rubbery state because of its low molecular weight. $T_{g, \text{gel}}$ represents the lowest isothermal cure temperature which will result in a material with elastomeric properties; below $T_{g, \text{gel}}$ the solid formed isothermally will be ungelled glass which on heating gives a viscous liquid (before further reaction occurs). Below $T_{g, \text{resin}}$ the resin remains as ungelled glass with essentially no chemical reactivity.

The remaining curve in Figure 5 is considered to represent an iso-viscosity contour. A rheological parameter often measured in thermosetting resins is the time to reach a particular viscosity (usually a function of the measurement technique) which is often identified as the gel point.

At the molecular level, isothermal cure of thermosetting systems is characterized by (molecular) gelation at a particular chemical conversion (8,9) (depending on the functionality of the reactants) and by a continual reduction of molecular mobility and chemical reactivity caused by increasing molecular weight and crosslinking. Extent of conversion contours (one of which is the gelation curve) on an isothermal molecular TTT cure diagram (Figure 6) indicate that the reaction becomes diffusion controlled and eventually quenched, regardless of whether or not gelation has occurred. The temperature at which the time to gel equals the time to vitrify is defined as $T_{g, \text{gel}}$; the resin will not gel below this temperature. This is related to the temperature $T_{g, \text{gel}}$ at which the liquid-to-rubber transition

disappears in the macroscopic TTT cure diagram.

Each point on the TTT cure diagrams represents a unique state, independent of the path by which it was attained, only if the system is homogeneous and the cure is limited to a single reaction path. If the system is non-homogeneous, phase separation (morphology and solubility) may be a function of the cure temperature. In a system where competing reactions exist the cure temperature will determine the favored reaction path. In the absence of these complications, an isocure path would follow the extent of conversion curve if the temperature were to change (10).

The molecular and macroscopic TTT diagrams are related in that the liquid-to-rubber transition is associated with gelation and the molecular T_g (quenching of reaction curve) is associated with vitrification (macroscopic T_g). The thermosetting process (cure) involves four states: liquid, gelled rubber, ungelled glass and gelled glass.

TTT cure diagrams can be used for studying chemical structure/physical property relationships because each system is unique with respect to both the kinetics of cure and the physical properties. In order to study structure/property relationships of thermosetting systems they must be cured above $T_{g\infty}$ to ensure that they have been fully cured. If they are not fully cured, their properties will depend on the extent of cure, as well as their chemical structure and morphology. The purpose of the present work is to use isothermal TTT cure diagrams and dynamic mechanical temperature scans of incompletely and fully cured systems as a basis for investigating structure/property relationships in epoxy/amine systems.

MATERIALS AND PROCEDURE

Each of a series of difunctional epoxies of the diglycidyl ether of bisphenol A type (i.e. Shell Epon 825, Epon 828, and Epon 834) was reacted with stoichiometric quantities (1 epoxy/1 amine hydrogen) of diaminodiphenylsulfone (DDS: Aldrich). The Epon 828 was also reacted separately with 4,4'-methylenedianiline (MDA: Aldrich), bis(p-aminocyclohexyl)methane (PACM-20: DuPont), and trimethyleneglycol di-p-aminobenzoate (TMAB: Polaroid). Their chemical structures are illustrated in Figure 7.

Macroscopic TTT cure diagrams were generated from torsion braid analysis (TBA) experiments in which the relative rigidity ($\alpha G'$), and logarithmic decrement (Δ) were obtained from the damped oscillations of the freely decaying torsion pendulum (~ 1 Hz). The supported specimens were made by dipping a glass braid in a solution of the epoxy and amine in methylethylketone, except in the case of Epon 828/PACM-20 which was applied neat since it is a liquid at room temperature. The specimens were then mounted in the TBA apparatus at the temperature of cure in a helium atmosphere and their moduli were monitored as a function of time. Transitions which occur during cure were identified by the maxima in the logarithmic decrement curves of the dynamic mechanical plots. Having cured the specimens until the reaction was quenched, as indicated by the levelling off of the modulus, thermomechanical spectra were obtained at 1.5°C/min. first cooling the specimen to -190°C and then heating it to 250°C to obtain the spectrum of the partially cured resin. The specimens were then cycled between 250°C and -190°C until there was no further change in T_g , indicating that the cure was complete. In this way $T_{g\infty}$, as well as the spectra of the fully cured resins were obtained for each cure temperature.

A typical isothermal plot (11) shown in Figure 8, displays three distinct processes. The elapsed time to each of these events is plotted vs. the isothermal cure temperature and in this way each of the curves on the macroscopic TTT cure diagram is generated. Examples of the thermomechanical spectra of the isothermally cured resin, and the subsequent fully cured resin are shown in Figure 9. Note that both the glassy state relaxation, T_{sec} , and T_g increase with increasing extent of cure, and that the rigidity of the undercured resin is greater than that of the fully cured resin in the region between T_{sec} and T_g (12, 13).

Dynamic viscosity, G' and G'' for Epon 828/PACM-20 were also obtained from oscillatory shear measurements at 1.6 Hz in a nitrogen atmosphere using a Rheometrics Dynamic Spectrometer. Samples were placed between parallel plates 25 mm in diameter, 0.5 mm apart and cured isothermally. The maxima in G'' and the preceding shoulder, as well as the two corresponding stages in G' (Figure 10) provide another set of rheological data which can also be plotted on the TTT diagram.

Extent of conversion data for the molecular TTT diagram have been obtained by IR techniques [Figure 11 (11, 14)] and, in principle, can also be obtained by differential scanning calorimetry (DSC) or titration. Theoretically, molecular gelation occurs at a specific extent of conversion. The gel point at any given temperature can be estimated from a plot of gel fraction vs. time, by noting the time at which the resin begins to be insoluble. The gel fractions of the isothermally curing resins were measured periodically by weighing the resin fraction insoluble in methylethylketone (dichloromethane for Epon 828/PACM-20). The gel fraction data for the Epon 828/PACM-20 system are shown in Figure 12: these occur between 70 and 80 per cent conversion (Figure 11). [The gel fraction experiments for the Epon 828/PACM-20

systems were performed on samples cured in a helium atmosphere. For Epon 825/DDS and Epon 834/DDS, gel fraction experiments were performed on samples cured in air. For Epon 828/DDS, in which cure was conducted both in air and helium, the gelation times were the same.]

RESULTS AND DISCUSSION

The dynamic mechanical (TBA) plots of the fully cured resins (Figure 13) show that whereas the glass transition temperature ($T_{g\infty}$) varies for each system, the broad secondary relaxation ($T_{sec\infty} < T_{g\infty}$) remains at approximately -40°C , indicating that it is probably due to localized backbone motion in the epoxy moiety which is common to all of these systems (12, 15, 16). The $T_{g\infty}$ of each resin was obtained by cycling between -190°C and 250°C until there was no further change in Tg. Figures 14-19 show T_{sec} and Tg for each of the resins cured isothermally until the modulus levels off, as well as $T_{sec\infty}$ and $T_{g\infty}$ of the fully cured resins, as a function of cure temperature. The Tg of the resin as identified by the maximum in the logarithmic decrement curve is higher than the cure temperature (as long as T_{cure} is below $T_{g\infty}$). At vitrification the rate of diffusion begins to dominate the kinetics of the reaction but the reaction is not quenched until the glass transition has risen well above the cure temperature. This difference between the glass transition temperature and the temperature at which molecular motion is quenched is evident in phenomena such as sub-Tg annealing, and predicted by theoretical expressions such as the WLF equation (17). The difference $T_g - T_{cure}$ varies with each resin system, and is tabulated in Table I along with values of T_{sec} , Tg, $T_{sec\infty}$ and $T_{g\infty}$.

Macroscopic TTT cure diagrams were obtained from TBA experiments for each of the six epoxy/amine systems. Rheological data using the Rheometrics Dynamic Spectrometer were obtained only for Epon 828/PACM-20, and gel fraction data were obtained for all except those cured with MDA and TMAB. Composite TTT diagrams are presented in Figures 20-25 consisting of the TBA, Rheometrics and gel fraction data. Activation energies, obtained by plotting the data in an Arrhenius fashion, are listed in Table II. With the exception of Epon 828/PACM-20 which is the only aliphatic amine cured system, the activation energies of the epoxy systems studied in this work were similar. Characteristic parameters of the TTT cure diagrams are listed in Table III; T_{gel} is the lowest temperature at which the resin gels, and T_{min} is the cure temperature at which the time to vitrify is a minimum.

The results fit the pattern of the macroscopic TTT cure diagram (Figure 5). In general the TBA results show three events, except for the Epon 828/DDS system in which the first event is missing.

The third event is associated with vitrification, as can be seen for example from the relative rigidity curve of Figure 8 which indicates a rubber-to-glass transition corresponding to the third maximum in logarithmic decrement. The entire S-shaped vitrification curve was obtained only for the Epon 828/PACM-20 system (Figure 24), since it was the only one in which a solvent was not required in sample preparation. The other systems all show the characteristic upper portion of the S-shaped curve. The G' data obtained from the Rheometrics Dynamic Spectrometer parallel the TBA relative rigidity data in the common temperature range that data were obtained. The lack of exact coincidence may be due to the transducer in the Dynamic Spectrometer approaching its upper limit.

The second event (Figure 8) can be associated with the liquid-to-rubber transition curve above T_{gel} . The modulus shows a corresponding rise from a liquid-to-rubbery state (Figures 8 and 10), and the Rheometrics data (Figure 10) show a shoulder in G'' which corresponds to the second event (TBA) in the Epon 828/PACM-20 system (Figure 8). Below T_{gel} , the shoulder in the Rheometrics Dynamic Spectrometer G'' data is not evident and G' shows only a liquid-to-glass transition. The TBA data exhibit the transition prior to vitrification over the entire temperature range; above T_{gel} it corresponds to the liquid-to-rubber transition, but between T_{resin} and T_{gel} it may^{or may not} be attributed to the composite nature of the specimen. A similar effect called the liquid-liquid transition (" T_{ll} ") has been observed in TBA measurements of amorphous thermoplastics (18) in^{which} at high molecular weights ($\bar{M}_n > M_c$, where M_c is the critical molecular weight for chain entanglement), this transition occurs at the onset of the rubbery plateau. It persists even at low molecular weight just as it does in the thermosetting resins.

The first event may be associated with an isoviscosity level. The interactions of the viscous liquid and the braid in a TBA experiment give rise to a maximum in logarithmic decrement, as the viscosity increases (19, 20). Other methods of monitoring the cure of thermosets (rising bubble, stirring motor, etc) identify (macroscopic) gelation with different viscosity levels.

Complementary Continuous Heating Transformation (CHT) cure diagrams were obtained by monitoring the dynamic mechanical properties of a thermosetting resin by TBA while raising the temperature at a series of constant rates. A temperature scan of a solid, initially unreacted, resin would be expected to reveal in sequence: Resin T_g , T_{ll} , an isoviscous event, an isoviscous event upon reaction, the liquid-to-rubber (or T_{ll})

transition, vitrification, devitrification and degradation. The isoviscous transitions would be observed only when the viscosity of the resin is below the isoviscous level. The scans in Figure 26 clearly show T_{resin} , T_{gel} , the liquid-to-rubber transition, and vitrification, in addition to another glass transition (devitrification) and a high temperature event corresponding to an intramolecular rearrangement reaction (11). The number of events observed depends on the heating rate; if the heating rate is too fast the vitrified state will be missed. The CHT diagram is generated by plotting the temperature vs. the time at which the events were observed. As one example, the CHT diagram for Epon 828/PACM-20 is shown in Figure 27.

Although the CHT diagram has the same features as the TTT cure diagram, albeit in a somewhat skewed form, it has a practical value. Most of the features of the CHT diagram, such as T_{resin} , T_{gel} and T_{∞} can be obtained from 3 to 4 temperature scans whereas many more are required for the TTT cure diagram. Furthermore, the choice of cure temperatures is more critical in the case of the TTT diagrams especially when the characteristic parameters of a system are unknown.

The results also fit the pattern of the molecular TTT cure diagram (Figure 6). The extent of conversion data obtained isothermally by FT-IR (Figure 11) for the Epon 828/PACM-20 system follow the trend indicated in Figure 6. As the extent of conversion curves approach the S-shaped glass transition curve they become horizontal lines as the reaction becomes diffusion controlled and ultimately is quenched. The gelation curve (determined from gel fraction data) lies parallel to the extent of conversion curves; and for Epon 828/PACM-20 lies between 70 and 80% extent of conversion. In the other systems for which gel fraction data were obtained, the gelation

curves follow the same form. For Epon 828/PACM-20 the lowest temperature at which gel fractions were obtained was 50°C whereas for the epoxy resins cured with DDS the lowest temperature was 102°C. The TTT cure diagrams show that the extrapolated gelation curve crosses the vitrification curve just below this temperature (50°C for PACM-20, 102°C for DDS), which corresponds to T_{gel}^{gel} in Figure 6.

The TTT cure diagrams indicate a correspondence between gelation and the liquid-to-rubber transition, as well as between $T_{gel}^{gel'}$ and T_{gel}^{gel} . Although the activation energies for the liquid-to-rubber transition are slightly less than those obtained for gelation (Table II), there is a close correlation between the two events. In the one case where an activation energy was obtained also by infrared, which might be considered to yield a more accurate value, the liquid-to-rubber transition provides a lower estimate whereas gelation (gel fraction) provides a higher estimate. A comparison of $T_{g_{\infty}}$ for the series of epoxies cured with DDS (Table I) indicates that $T_{g_{\infty}}$ is quite sensitive to the length of the epoxy molecule, i.e. the distance between crosslinks. As the molecular weight of the epoxy monomer increases [as n (Figure 7) increases from 0 to 0.6] $T_{g_{\infty}}$ changes from 220°C to 185°C. On the other hand, $T_{g_{\infty}}$ is rather insensitive to the flexibility of the curing agent. One would expect the flexibility to increase in the order: MDA < PACM-20 < TMAB, but $T_{g_{\infty}}$ is approximately the same (165°C) for all of them. The difference in $T_{g_{\infty}}$ for Epon 828/DDS and Epon 828/MDA, Epon 828/PACM-20, or Epon 828/TMAB can be attributed to the polarity of the DDS moiety and its capability of being a site for hydrogen bonding, which could increase the apparent crosslink density thereby giving rise to the higher glass transition temperature.

The difference in the reactivity of the curing agents is also demonstrated in the TTT diagrams. Although the energy of activation, E_a , (Table II) as determined from gelation data, is practically the same for all but one of the curing agents investigated in this work, the rates of reaction vary widely. This can be seen from the horizontal shift in the gelation and vitrification curves. The curing agents ranked in order of decreasing reactivity are: DDS < TMAB < MDA < PACM-20.

The chemical reactivity, as well as the value of Tg_∞ , influence the sharpness of the upper portion of the TTT diagram, of which $Tg_\infty - \min Tg$ (Table III) is a measure.

CONCLUSION

The curing process can be understood in terms of the molecular and macroscopic TTT cure diagrams, as the complex interaction of chemical reaction and changing physical properties. No single technique exists with which one could extract both macroscopic and molecular level information from a thermosetting system. However, a series of isothermal TBA experiments can provide a qualitative description of a system's TTT cure diagram, including Tg_{resin} , Tg_∞ , the S-shaped vitrification curve, and, through the correlation of the liquid-to-rubber transition with gelation, Tg_{gel} . This procedure has been used to compare various amine-cured epoxy systems from the point of view of structure/property relationships.

ACKNOWLEDGMENT

Partial support was provided by the Chemistry Branch of the Office of Naval Research.

LITERATURE CITED

1. Gillham, J. K., *AIChE Journal*, 1974, 20, 1066.
2. Gillham, J. K., *Polymer Engineering and Science*, 1979, 19, 676.
3. Gillham, J. K., "Torsional Braid Analysis (TBA) of Polymers", in Developments in Polymer Characterization - 3, J. V. Dawkins, Ed., Applied Science Publishers, London, 1982. Ch. 5.
4. National Materials Advisory Board Publication 356 (1981), "Organic Matrix Structural Composites: Quality Assurance and Reproducibility", Ch. 3.
5. American Society for Testing and Materials, Philadelphia, PA, USA.
6. Gillham, J. K.; Stadnicki, S. J.; Hazony, Y., *J. Appl. Polymer Sci.*, 1977, 21, 40.
7. Enns, J. B.; Gillham, J. K., "Computer Applications in Coatings and Plastics", ACS Symposium Series (1982).
8. Flory, P. J., Principles of Polymer Chemistry, Cornell University Press, Ithaca, 1953.
9. Lunak, S.; Vladyka, J.; Dusek, K., *Polymer*, 1978, 19, 931.
10. Lee, C. Y-C.; Goldfarb, I. J., *Polymer Engineering and Science*, 1981, 21, 951.
11. Enns, J. B., Ph.D. Thesis, Princeton Univ. 1982.
12. Hartman, B.; Lee, G. F., *J. Appl. Polymer Sci.*, 1977, 21, 1341.
13. Aherne, J. P.; Enns, J. B.; Doyle, M. J.; Gillham, J. K., *Amer. Chem. Soc., Division of Organic Coatings and Plastics Chemistry, Preprints*, 1982, 46, 574.
14. Enns, J. B.; Gillham, J. K.; Small, R., *Amer. Chem. Soc., Polymer Division Preprints*, 1981, 22, 123.
15. Arridge, R. G. C.; Speake, J. H.; *Polymer*, 1972, 13, 450.
16. Pogany, G. A., *Polymer*, 1970, 11, 66.
17. Billmeyer, F. R., Textbook of Polymer Science, J. Wiley, N.Y., 1971.
18. Gillham, J. K., *Polymer Engineering and Science*, 1979, 19, 749.
19. Nielsen, L. E., *Polymer Engineering and Science*, 1977, 17, 713.
20. Neumann, B. M.; Senich, G. A.; MacKnight, W. J., *Polymer Engineering and Science*, 1978, 18, 624.

TABLE I. Cured Resins (Figures 14-19): Characteristic Parameters

	T_{sec} (°C)	Tg_{∞} (°C)	$Tg - T_{\text{cure}}$ (°C)
Epon 825/DDS	-35	220	24
Epon 828/DDS	-35	210	25
Epon 834/DDS	-37	185	20
Epon 828/MDA	-50	168	30
Epon 828/PACM-20	-33	165	30
Epon 828/TMAB	-40	166	24

TABLE II. Activation Energies (Figures 20-25)

	E_a^* (isoviscous) kcal/mole	E_a^* (liquid-to-rubber) kcal/mole	E_a^{\dagger} (gel) kcal/mole	$E_a^{\#}$ kcal/mole
Epon 825/DDS	11.5	14.8	16.6	—
Epon 828/DDS	—	14.3	16.3	—
Epon 834/DDS	10.0	14.0	15.7	—
Epon 828/MDA	13.6	15.4	—	—
Epon 828/PACM-20	8.5	10.7	16.8	12.6
Epon 828/TMAB	12.2	13.7	—	—

*TBA

†gel fraction

infrared (11)

TABLE III. TTT Cure Diagrams (Figures 20-25): Characteristic Parameters

	gel Tg (time) °C (min)	min Tg (time) °C (min)	$Tg_{\infty} - \text{min } Tg$ °C
Epon 825/DDS	100 (1000)	200 (63)	20
Epon 828/DDS	100 (1000)	205 (30)	5
Epon 834/DDS	100 (1000)	170 (425)	15
Epon 828/MDA	—	130 (35)	38
Epon 828/PACM-20	50 (165)	130 (10)	35
Epon 828/TMAB	—	140 (300)	27

FIGURE CAPTIONS

- Figure 1. Automated torsion pendulum: schematic. An analog electrical signal results from using a light beam passing through a pair of polarizers, one of which oscillates with the pendulum. The pendulum is aligned for linear response and initiated by a computer that also processes the damped waves to provide the elastic modulus and mechanical damping data, which are plotted on an XYY plotter versus temperature or time.
- Figure 2. Automated torsion pendulum: photograph of apparatus (see text).
- Figure 3. Automated torsion pendulum: system schematic for interfacing with a digital computer. The torsion pendulum has been interfaced with a digital desktop computer (HP-9825B). The motors which align the specimen and initiate the waves are under computer control. The wave and amplified analog thermo-couple signals reach the computer digitized via a digital voltmeter (HP-3437A). The scanner (HP-3495A) supervises the I/O activity. Upon receiving the digitized raw data the computer calculates the frequency and damping parameters, and plots the dynamic mechanical properties of the specimen as a function of temperature and time.
- Figure 4. Automated torsion pendulum: control sequence. I) Previous wave decays, drift detected and correction begins. II) Reference level of polarizer pair reached. III) Wave initiating sequence begins. IV) Decay of transients. V) Free oscillations begin. VI) Data collected. VII) Control sequence repeated.

- Figure 5. Macroscopic TTT cure diagram.
- Figure 6. Molecular TTT cure diagram.
- Figure 7. Chemical structures of epoxy resins and amine curing agents.
- Figure 8. Isothermal cure of a thermosetting epoxy (TBA): Epon 828/TMAB at 80°C. In general three events are discerned, the last being vitrification, and the second gelation. Times to each of these events are measured for different isothermal temperatures as a basis for generating a Time-Temperature-Transformation cure diagram for the particular thermosetting system (see Figures 20-25).
- Figure 9. Dynamic mechanical spectra of Epon 828/TMAB cured at 80°C. Spectrum A is obtained on cooling to -190°C after isothermal cure (80°C) (see Figure 8). Spectrum B is obtained after heating to 250°C to completely cure the resin.
- Figure 10. Dynamic mechanical data (Rheometrics), G' and G'', obtained by isothermally curing Epon 828/PACM-20 at several temperatures.
- Figure 11. Extent of conversion data obtained by monitoring the ratio of the 1184 cm^{-1} and 915 cm^{-1} peaks in the FT-IR spectrum of Epon 828/PACM-20 as a function of time at different temperatures, superimposed on the gelation and vitrification curves of the TTT cure diagram for that system (Figure 24).
- Figure 12. Gel fraction data for Epon 828/PACM-20. Gel points were obtained by monitoring the gel fraction of the resin during cure in a helium atmosphere.

Figure 13. TBA spectra of fully cured epoxy systems:

- a) relative rigidity
- b) logarithmic decrement.

Specimens were cured isothermally (at the designated temperature) and post-cured by cycling to 250°C.

Figure 14. T_{sec} and T_g as a function of cure temperature for Epon 825/DDS.
*as cured, †post-cured.

Figure 15. T_{sec} and T_g as a function of cure temperature for Epon 828/DDS.
*as cured, †post-cured.

Figure 16. T_{sec} and T_g as a function of cure temperature for Epon 834/DDS.
*as cured, †post-cured.

Figure 17. T_{sec} and T_g as a function of cure temperature for Epon 828/MDA.
*as cured, †post-cured.

Figure 18. T_{sec} and T_g as a function of cure temperature for Epon 828/PACM-20.
*as cured, †post-cured.

Figure 19. T_{sec} and T_g as a function of cure temperature for Epon 828/TMAB.
*as cured, †post-cured.

Figure 20. TTT cure diagram of Epon 825/DDS, including TBA and gel fraction data.

Figure 21. TTT cure diagram of Epon 828/DDS, including TBA and gel fraction data.

Figure 22. TTT cure diagram of Epon 834/DDS, including TBA and gel fraction data.

Figure 23. TTT cure diagram of Epon 828/MDA, TBA data.

Figure 24. TTT cure diagram of Epon 828/PACM-20, including TBA, Rheometrics, and gel fraction data.

Figure 25. TTT cure diagram of Epon 828/TMAB, TBA data.

Figure 26. Temperature Scans of Epon 828/PACM-20 from -50°C to 275°C at various scanning rates: a) relative rigidity; b) logarithmic decrement.

Figure 27. CHT diagram of Epon 828/PACM-20: temperature scans were performed at 0.05, 0.1, 0.2, 0.5, 1.0, 1.5, 2.0, and $4.0^{\circ}\text{C}/\text{min}$. from -50°C to 275°C .

Symbols: Δ vitrification;

\circ liquid-to-rubber transition;

\square isoviscous phenomenon;

* intramolecular rearrangement.

Note that heating rates greater than $2^{\circ}\text{C}/\text{min}$ are required to cure the resin without the occurrence of vitrification.

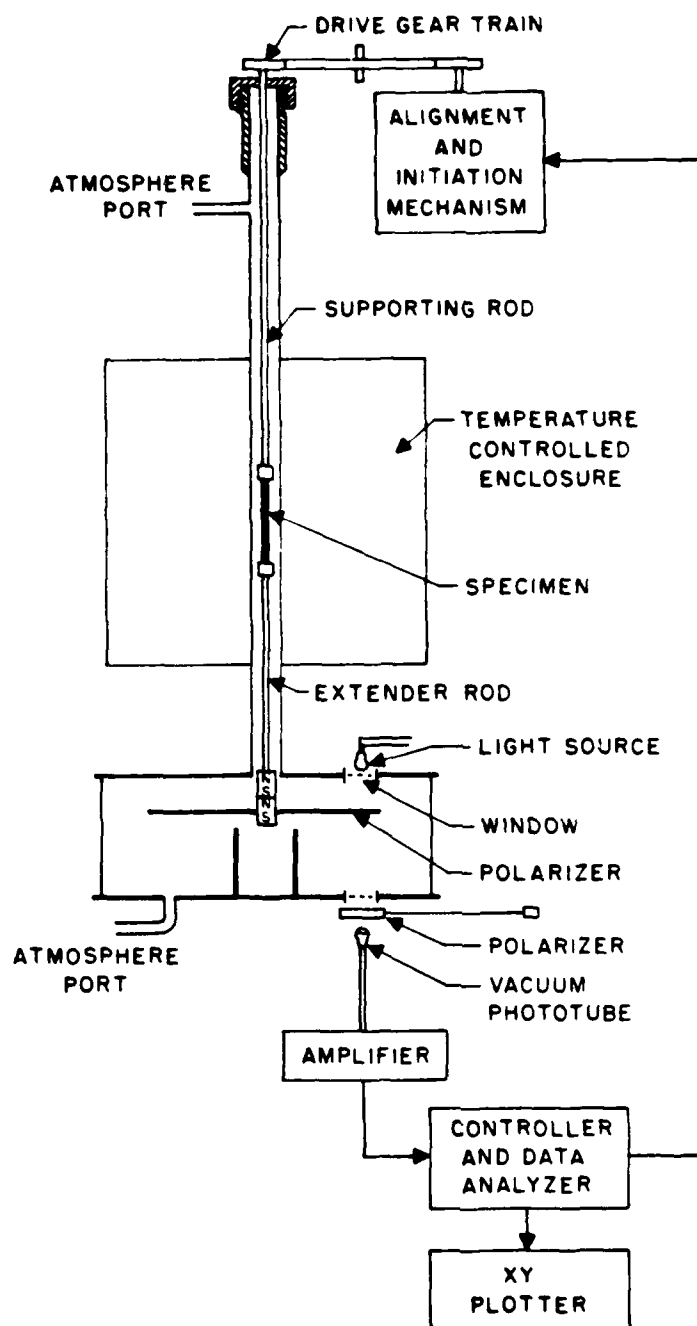


Fig. 1

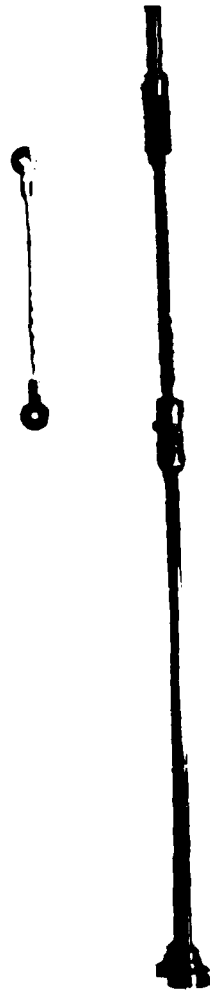
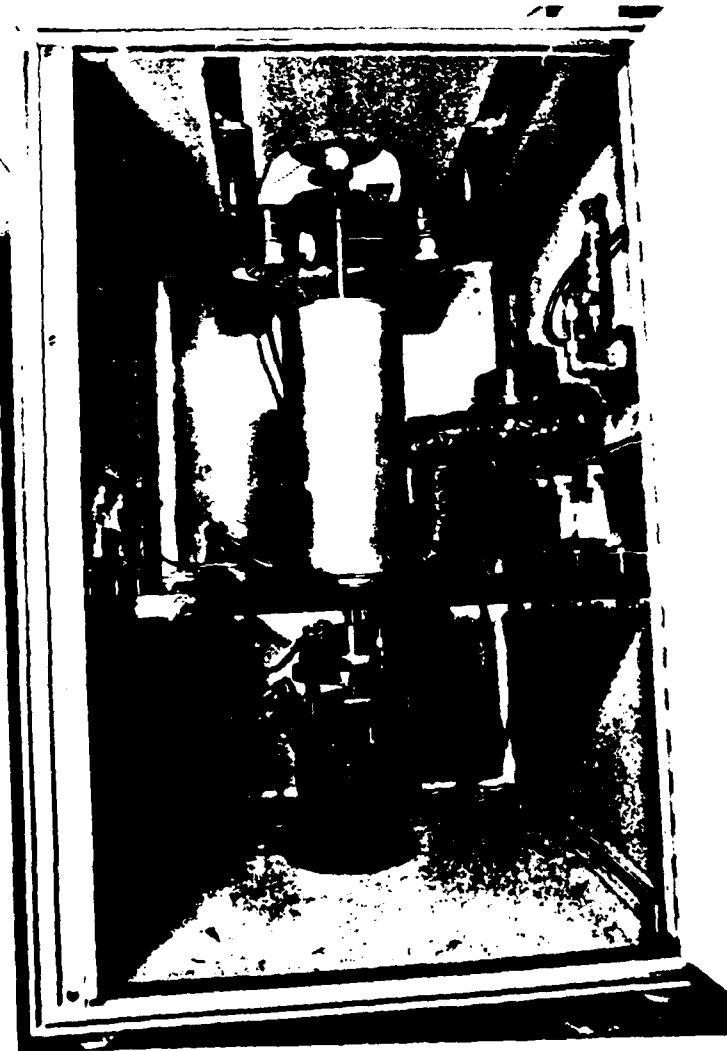
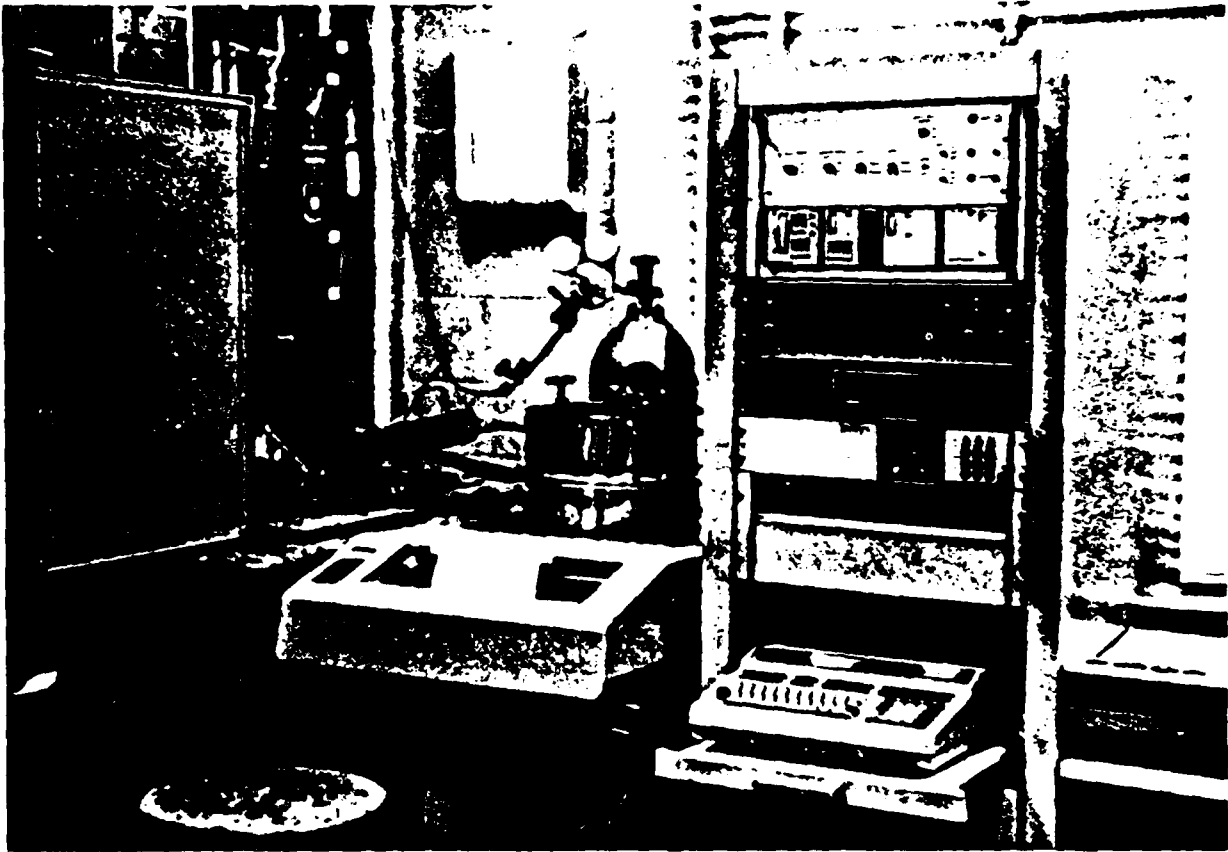


Figure 2

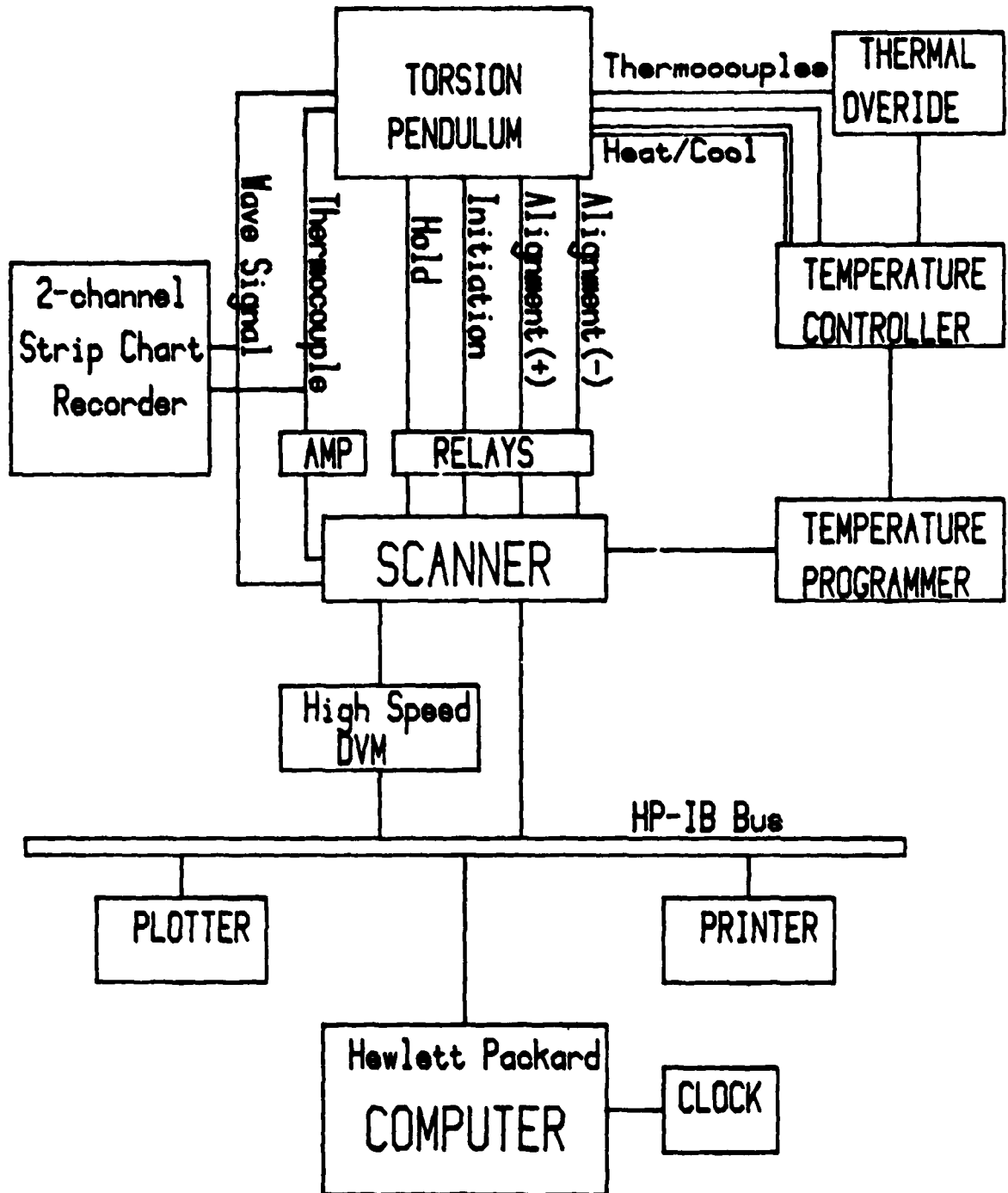
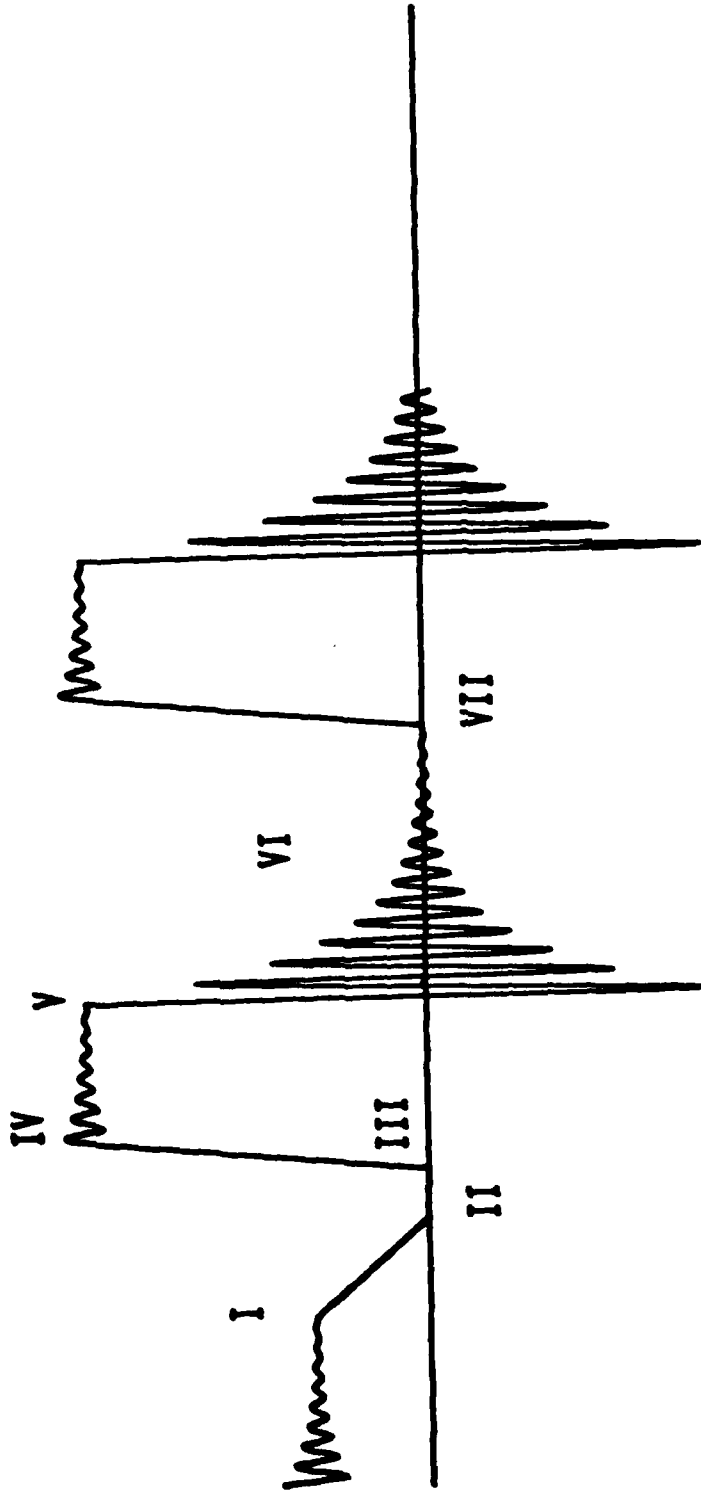


Fig. 3

CONTROL SEQUENCE



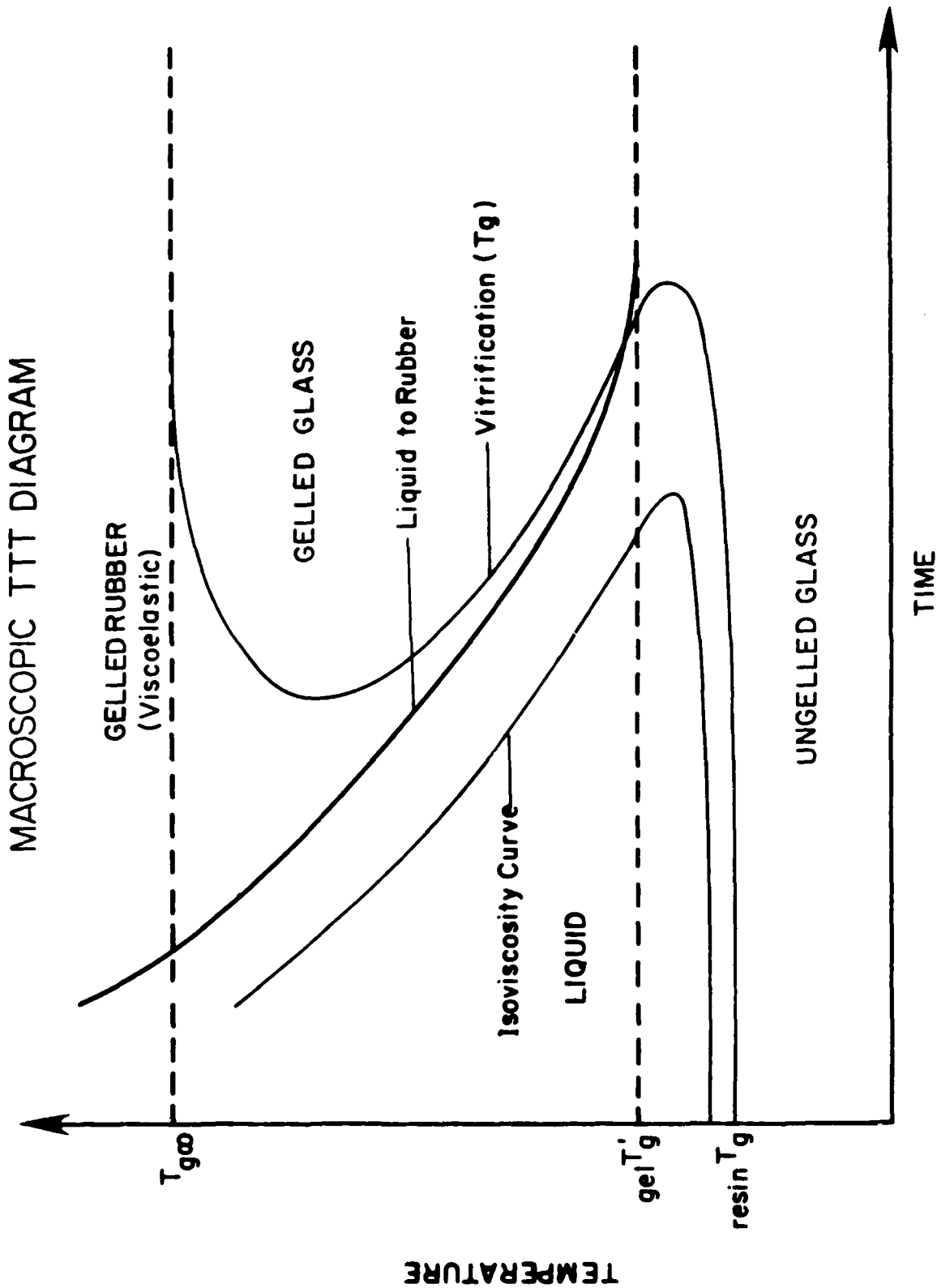


Fig. 5

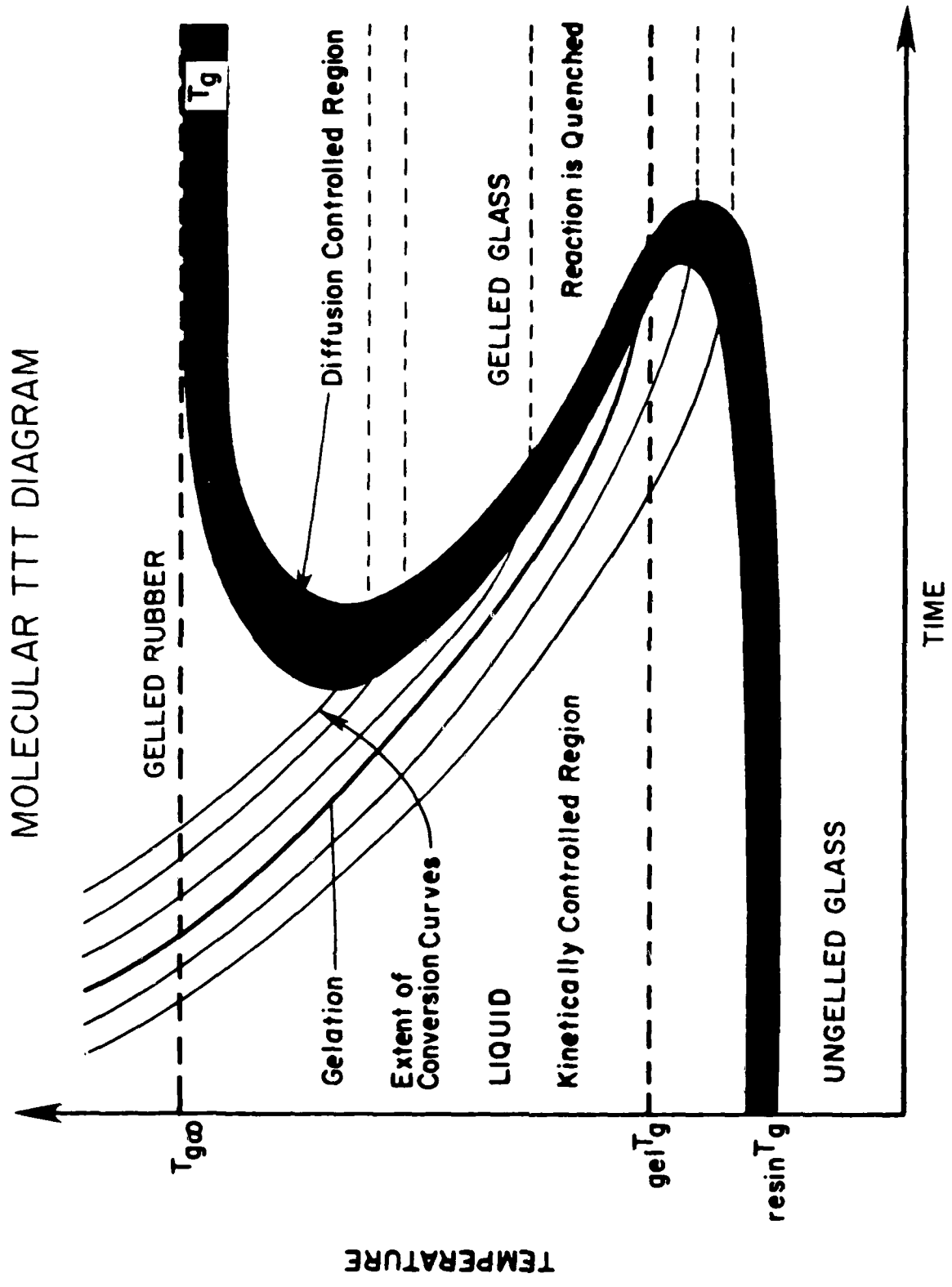
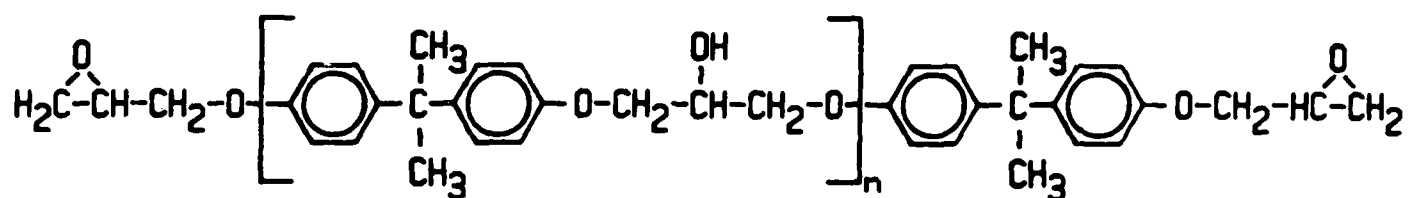


Fig. 6

EPOXY: Diglycidyl Ether of Bisphenol A

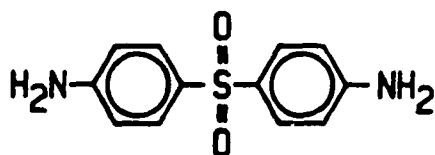


Epon 825: $n = 0$

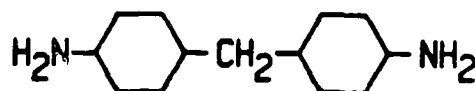
Epon 828: $n = 0.15$

Epon 834: $n = 0.6$

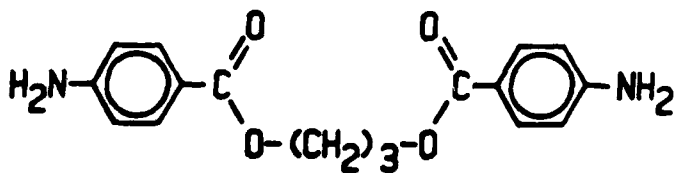
AMINE CURING AGENTS



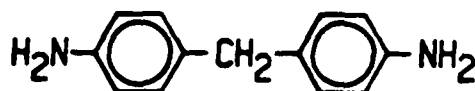
4,4'-Diaminodiphenyl Sulfone
(DDS)



Bis(p-aminocyclohexyl)methane
(PACM-20)



Trimethylene glycol
di-p-aminobenzoate (TMAB)



4,4'-Methylenedianiline
(MDA)

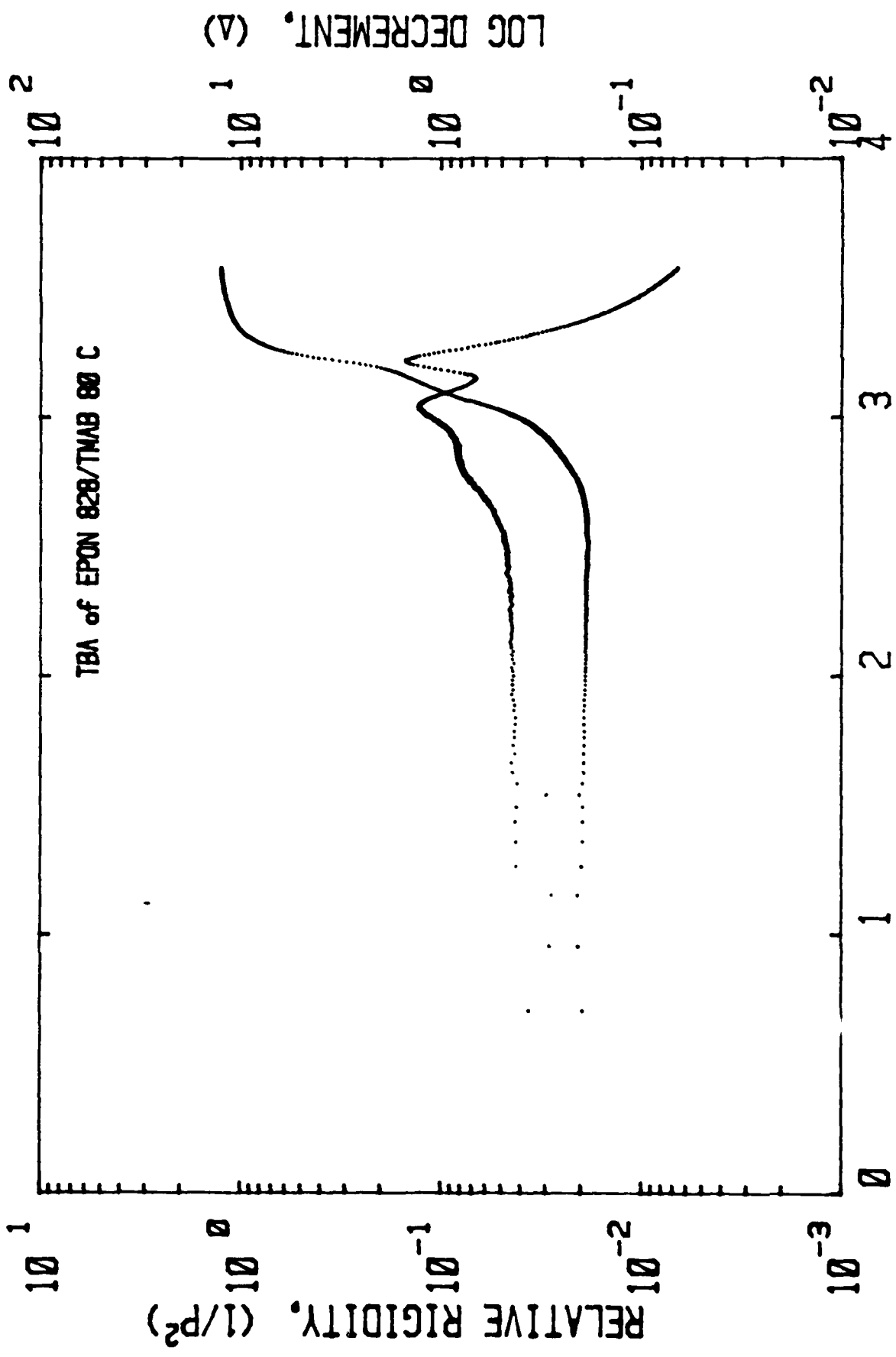


FIG. 8

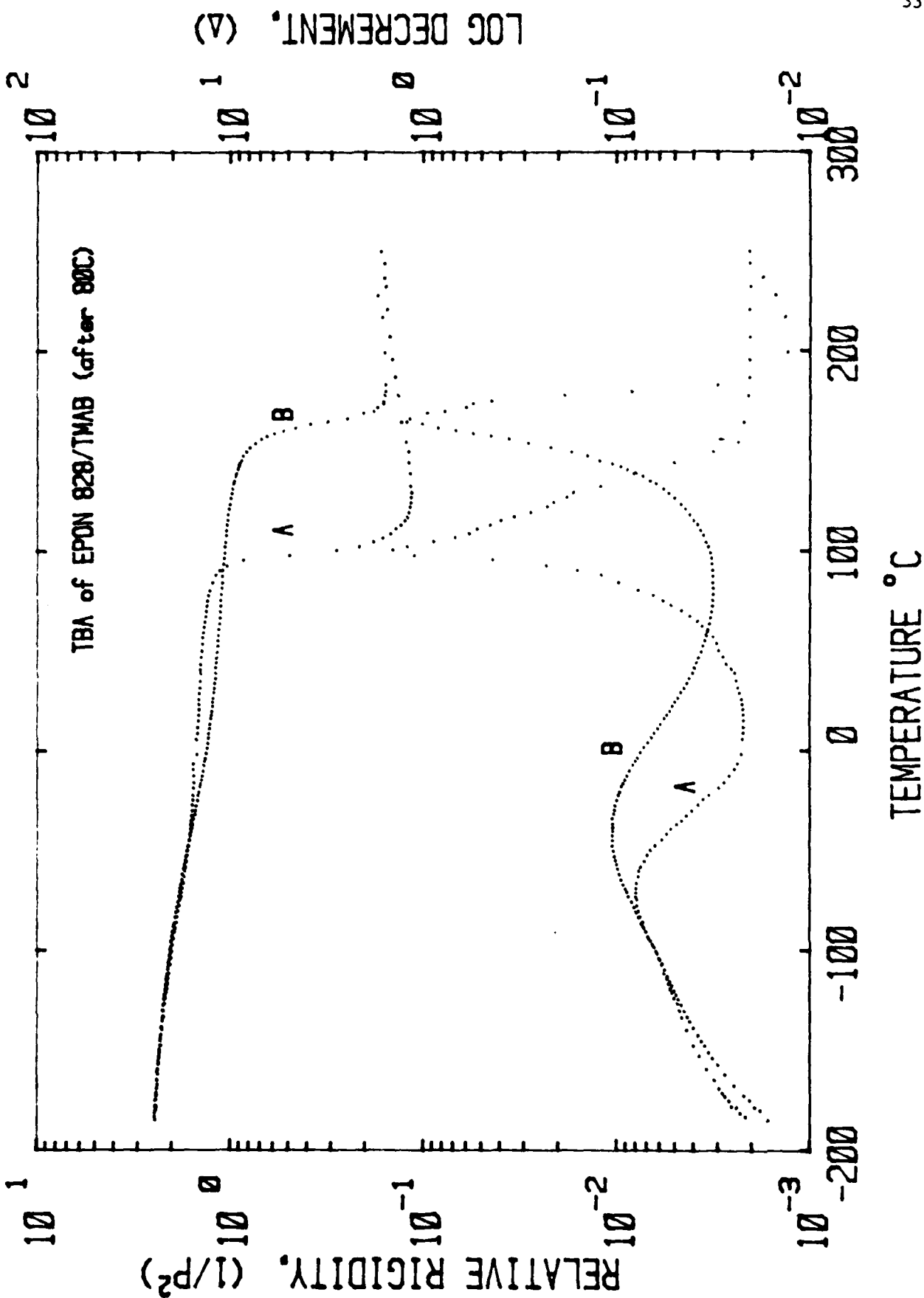


FIG. 9

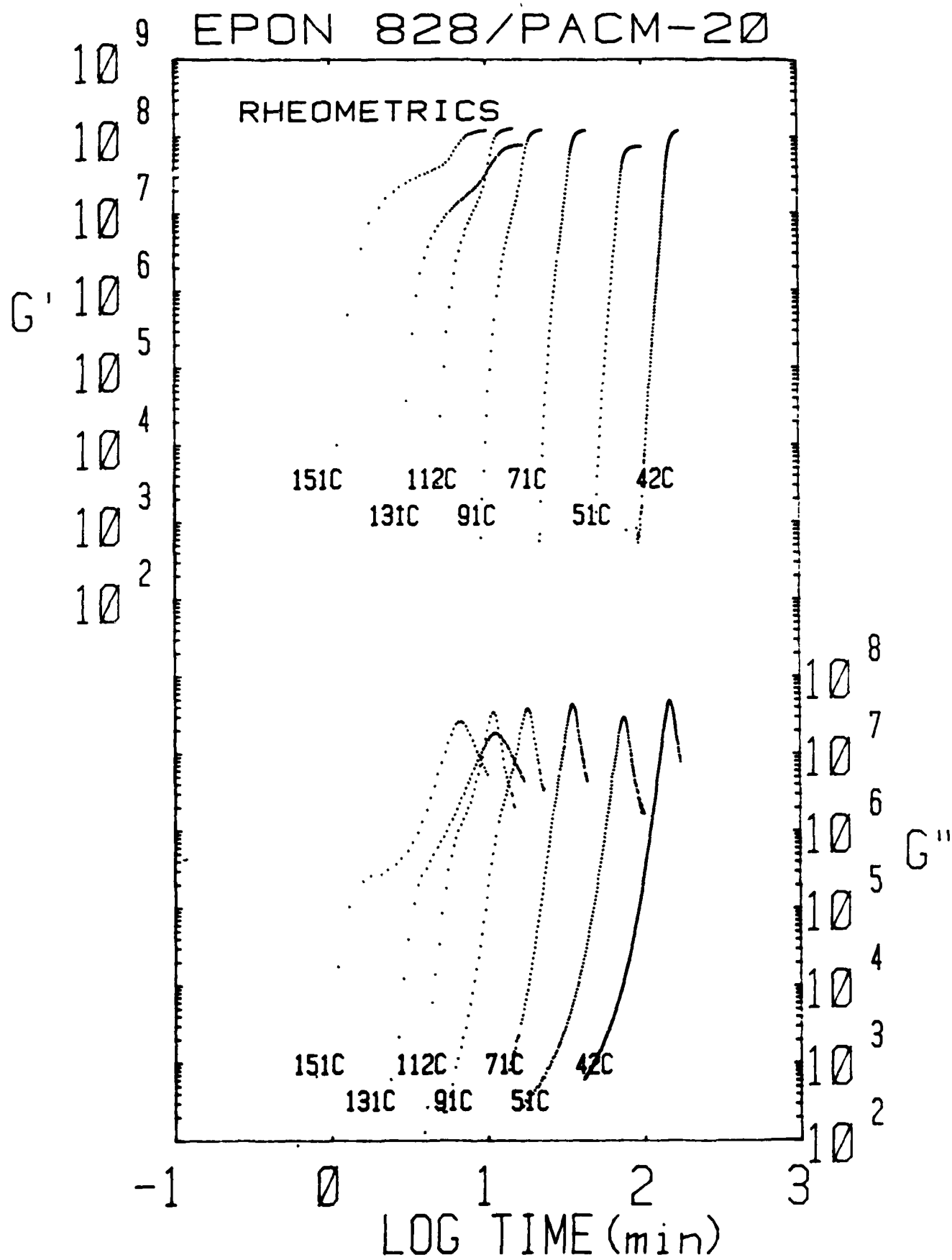


Fig. 10

EXTENT OF CONVERSION: FT-IR

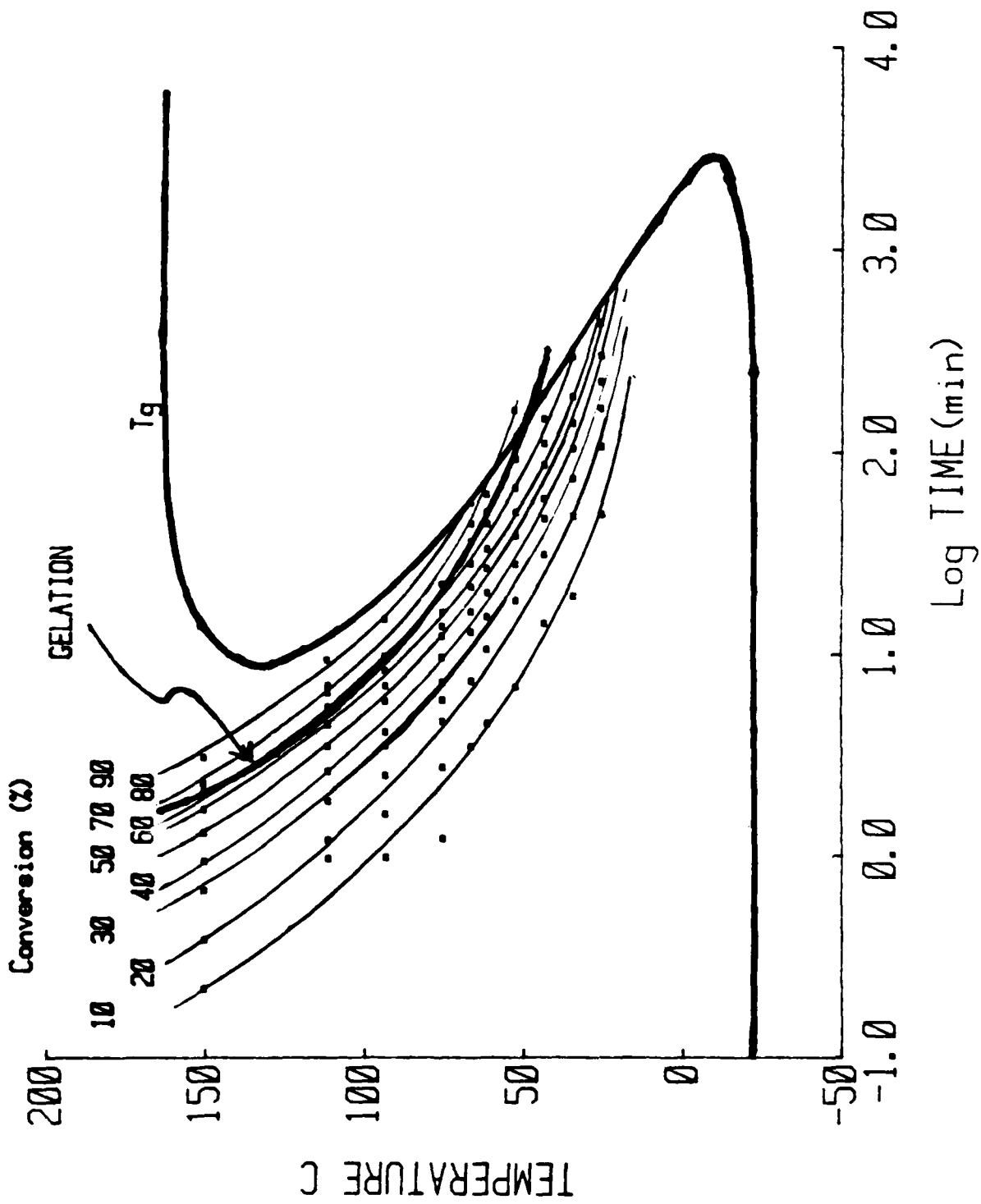


FIG. 11

EPON 828/PACM-20

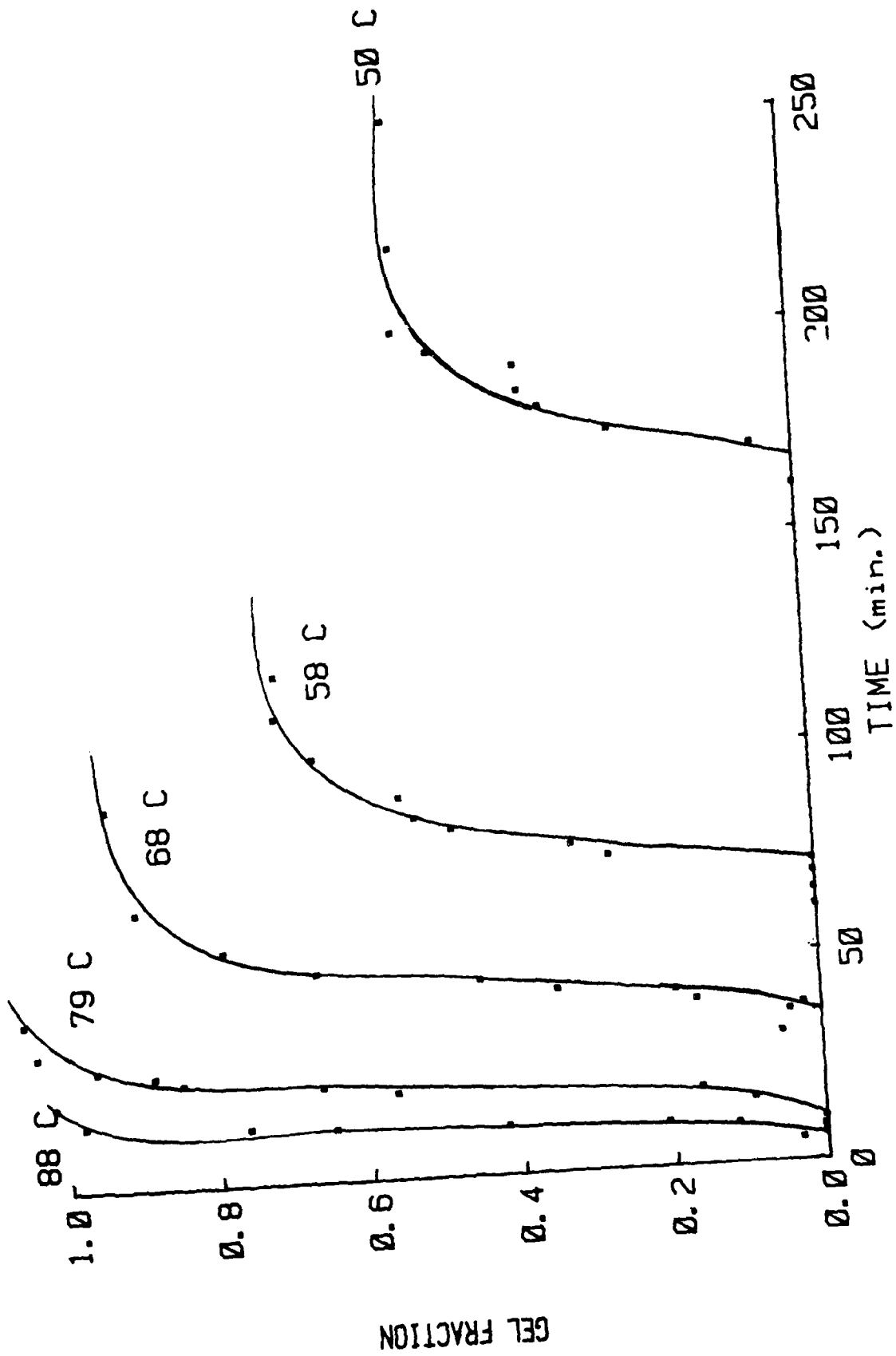


Fig. 12

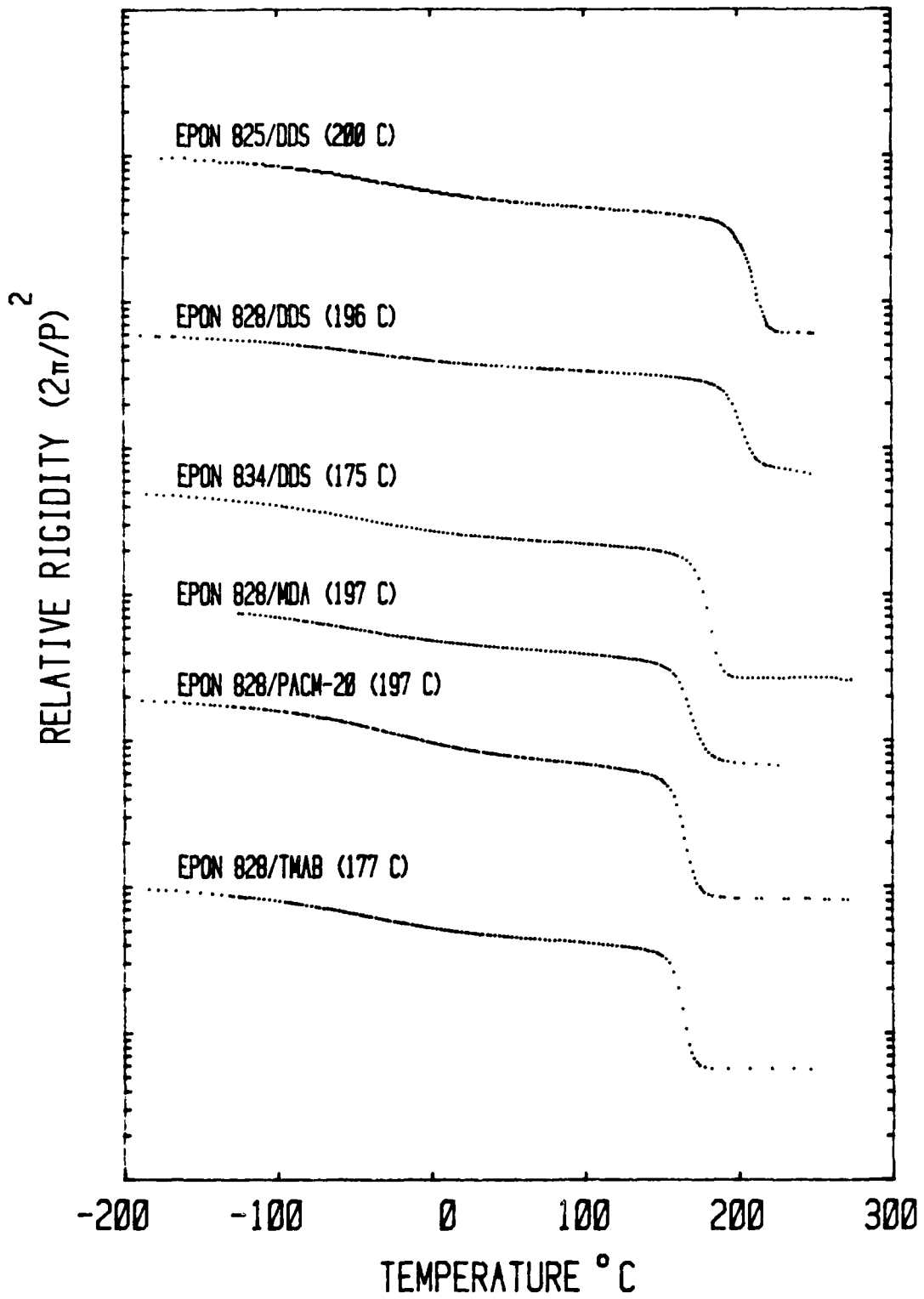


Figure 13A

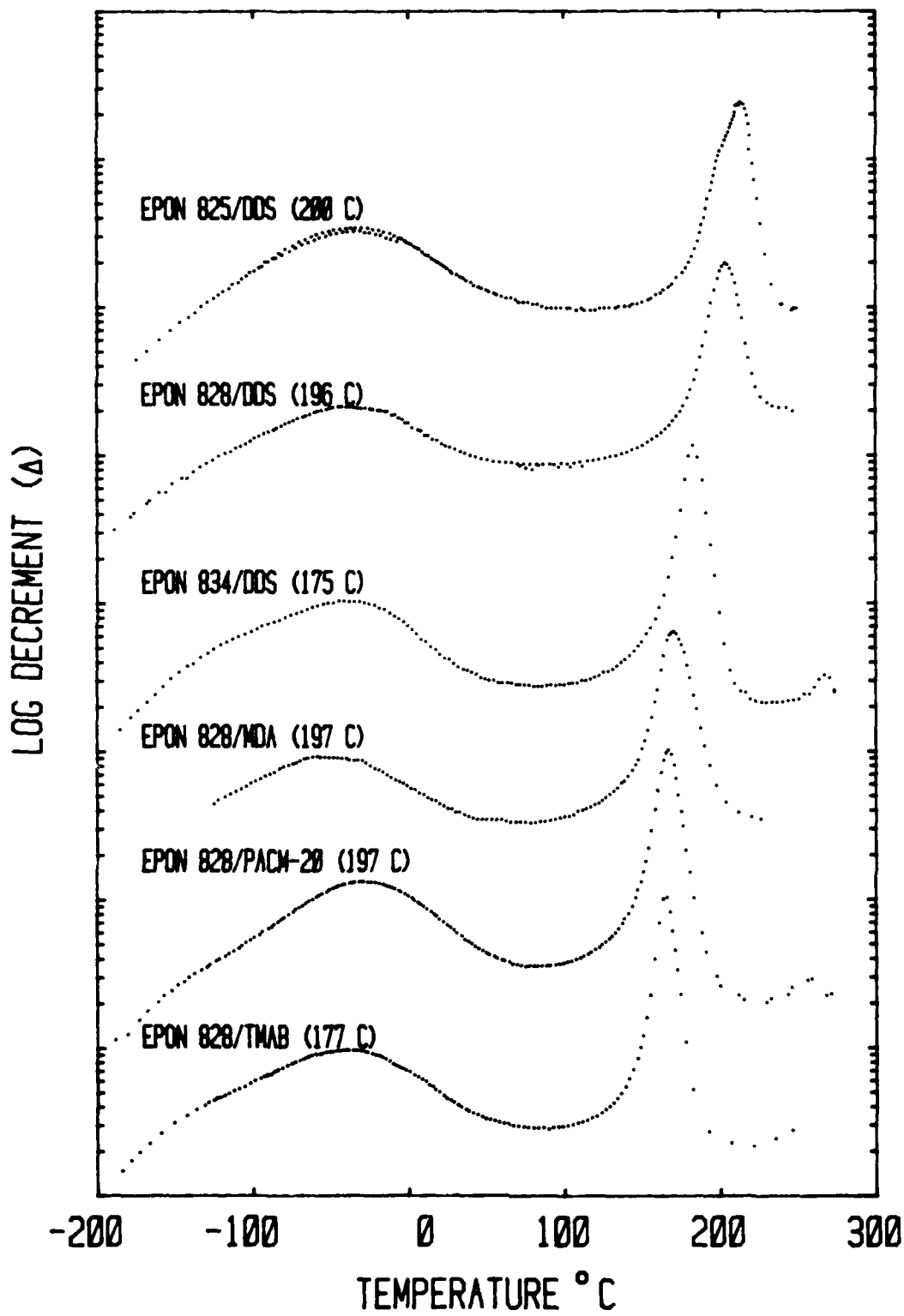


Figure 13B

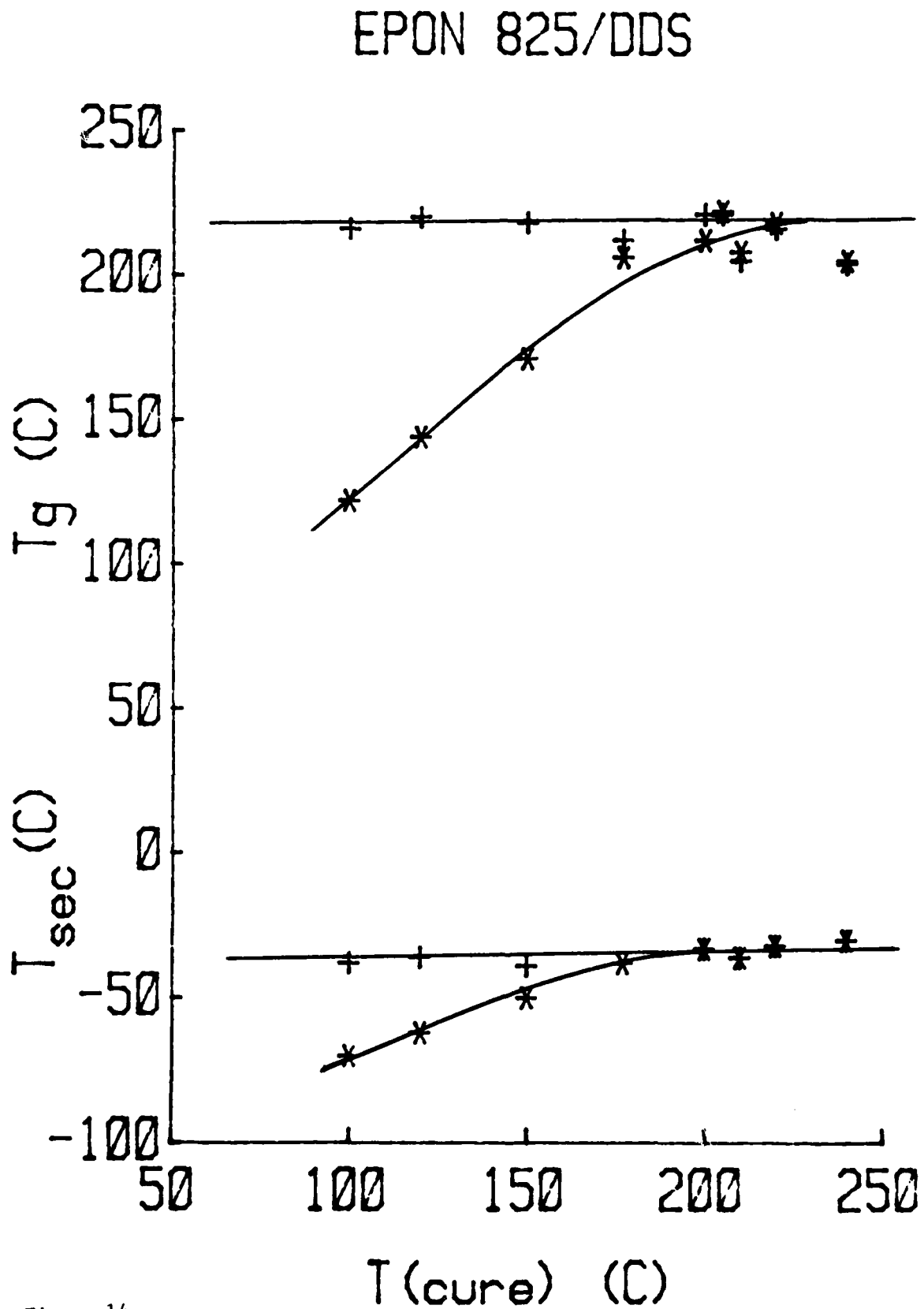


Figure 14

EPON 828/DDS

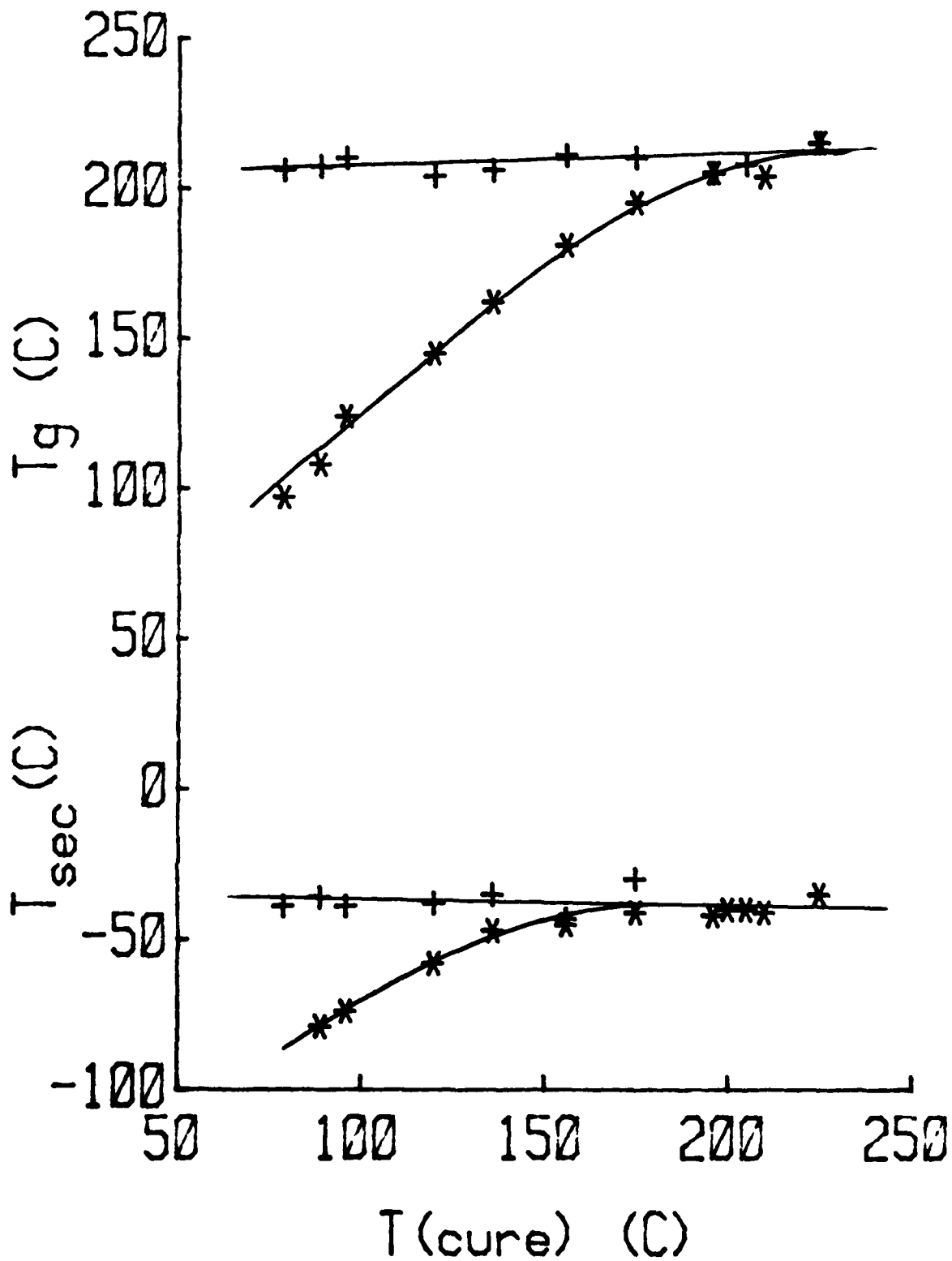


Figure 15

EPON 834/DDS

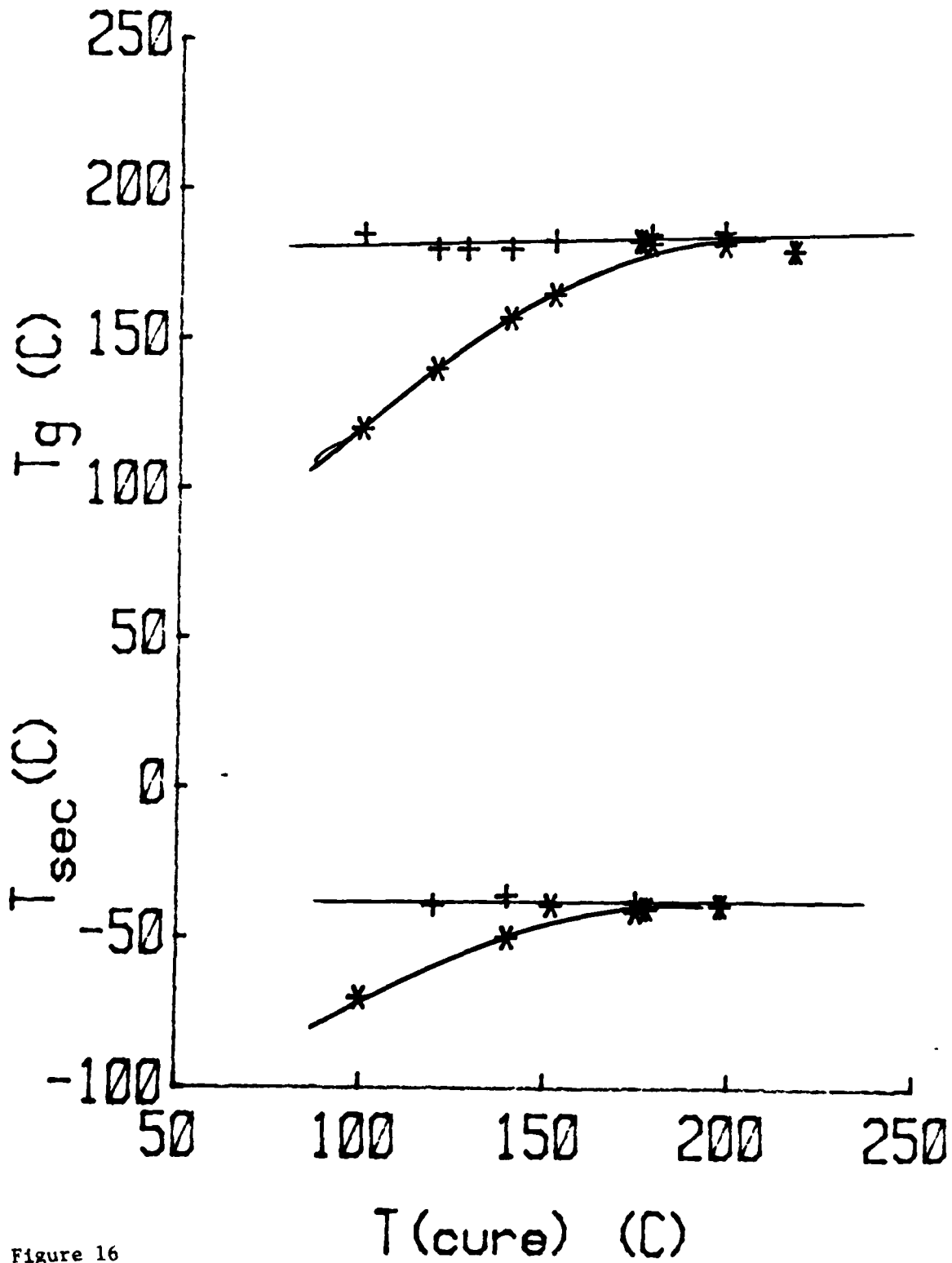


Figure 16

EPON 828/MDA

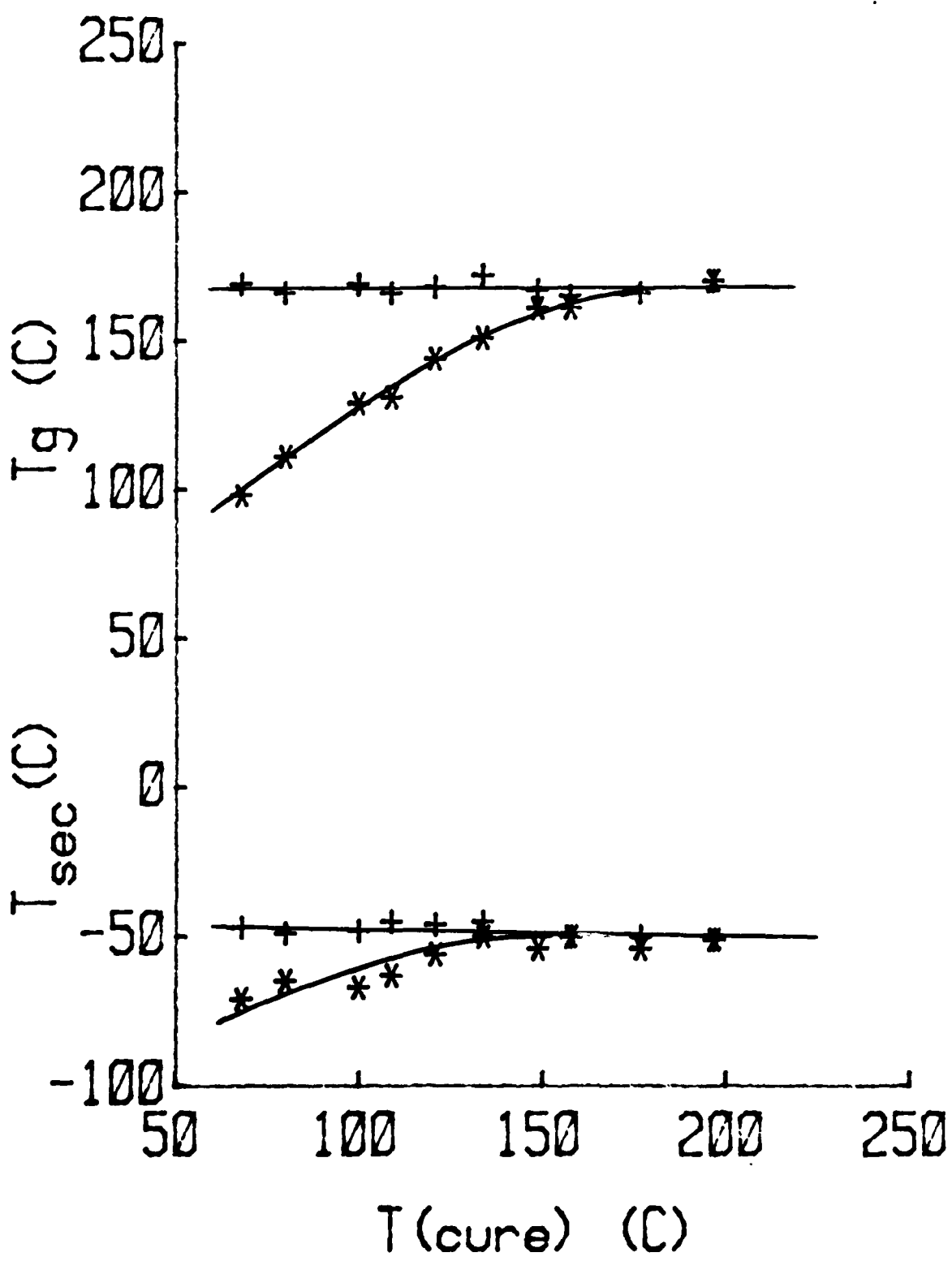


Figure 17

EPON 828/PACM-20

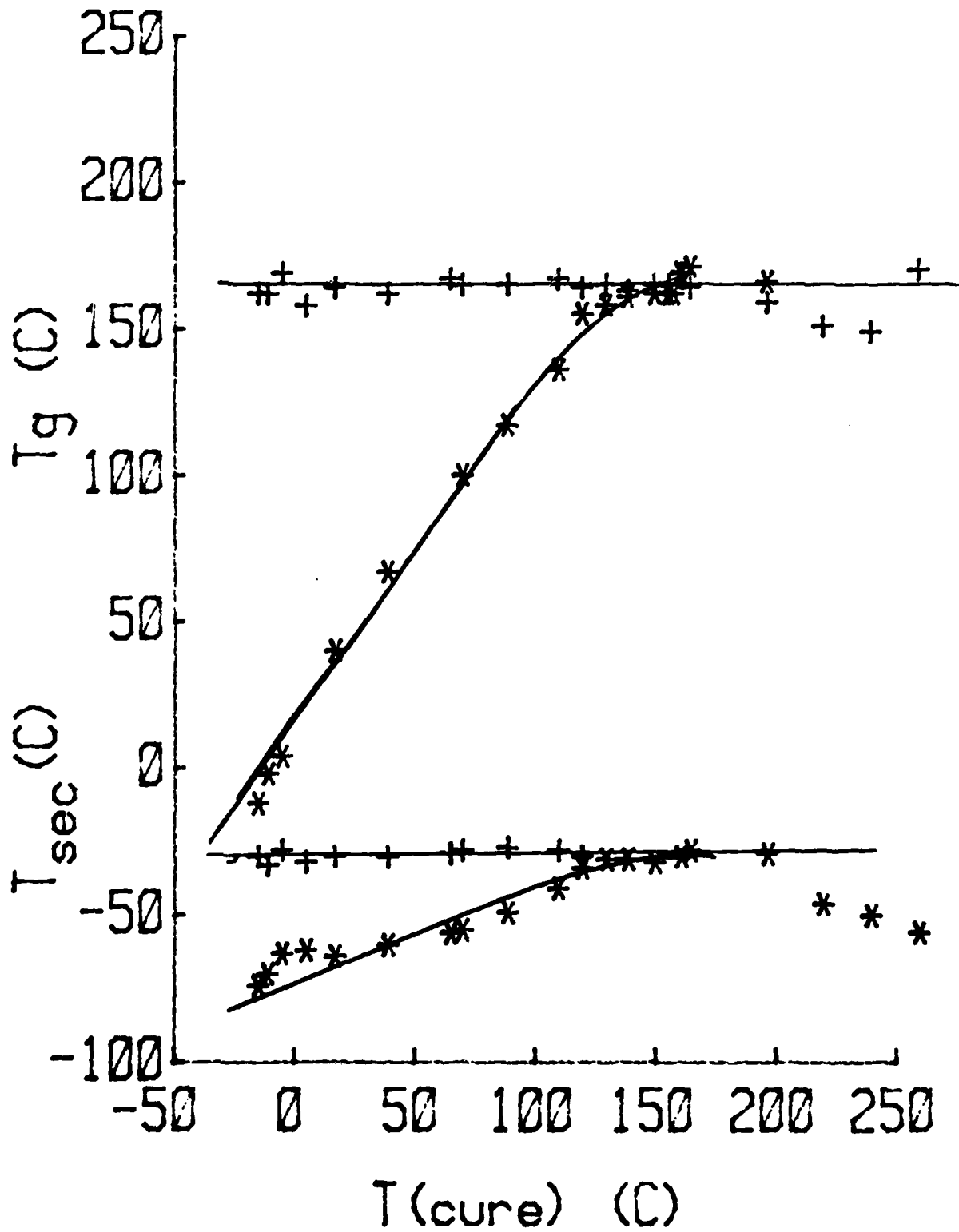


Figure 18

EPON 828/TMAB

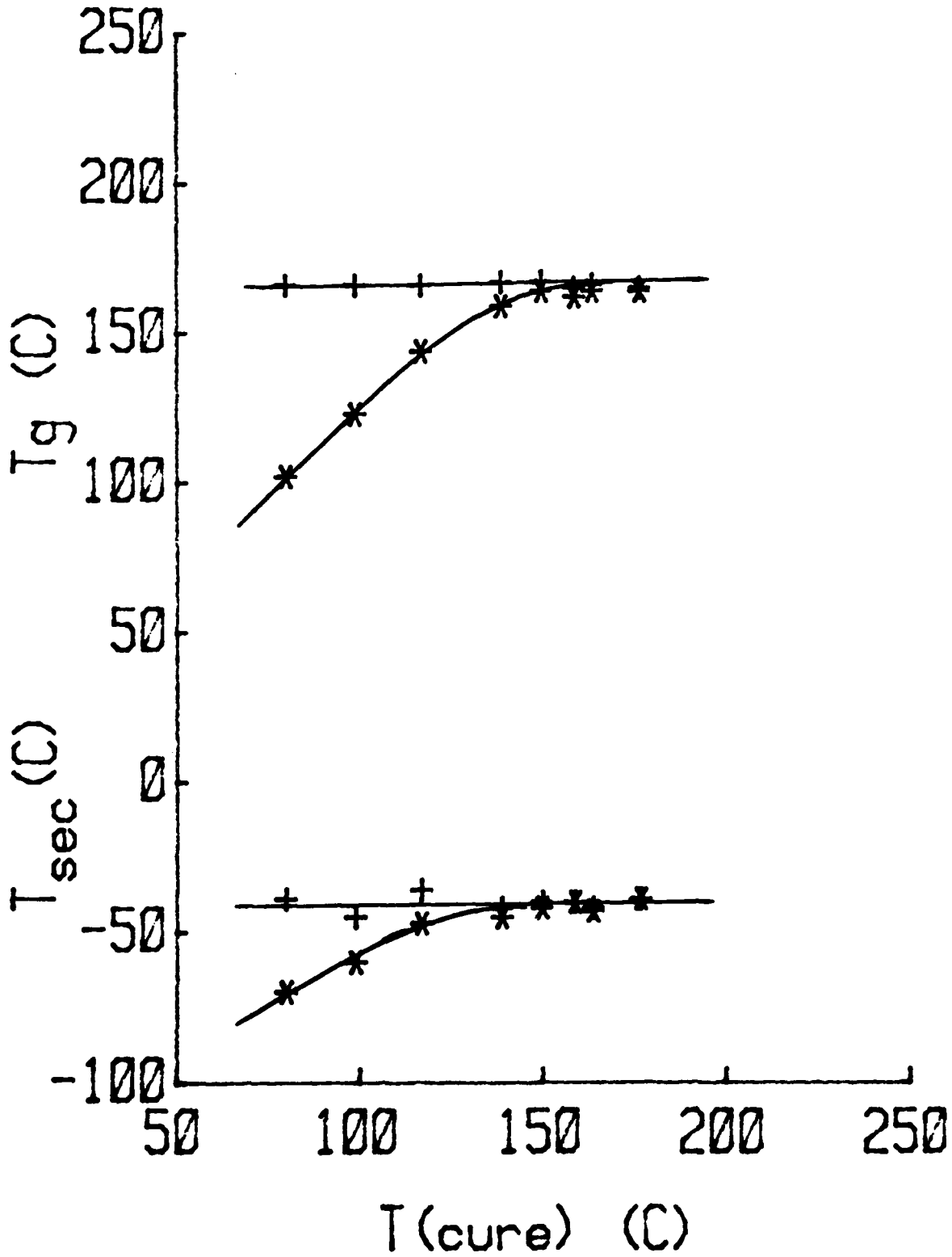


Figure 19

TTT DIAGRAM: EPON 825/DDS

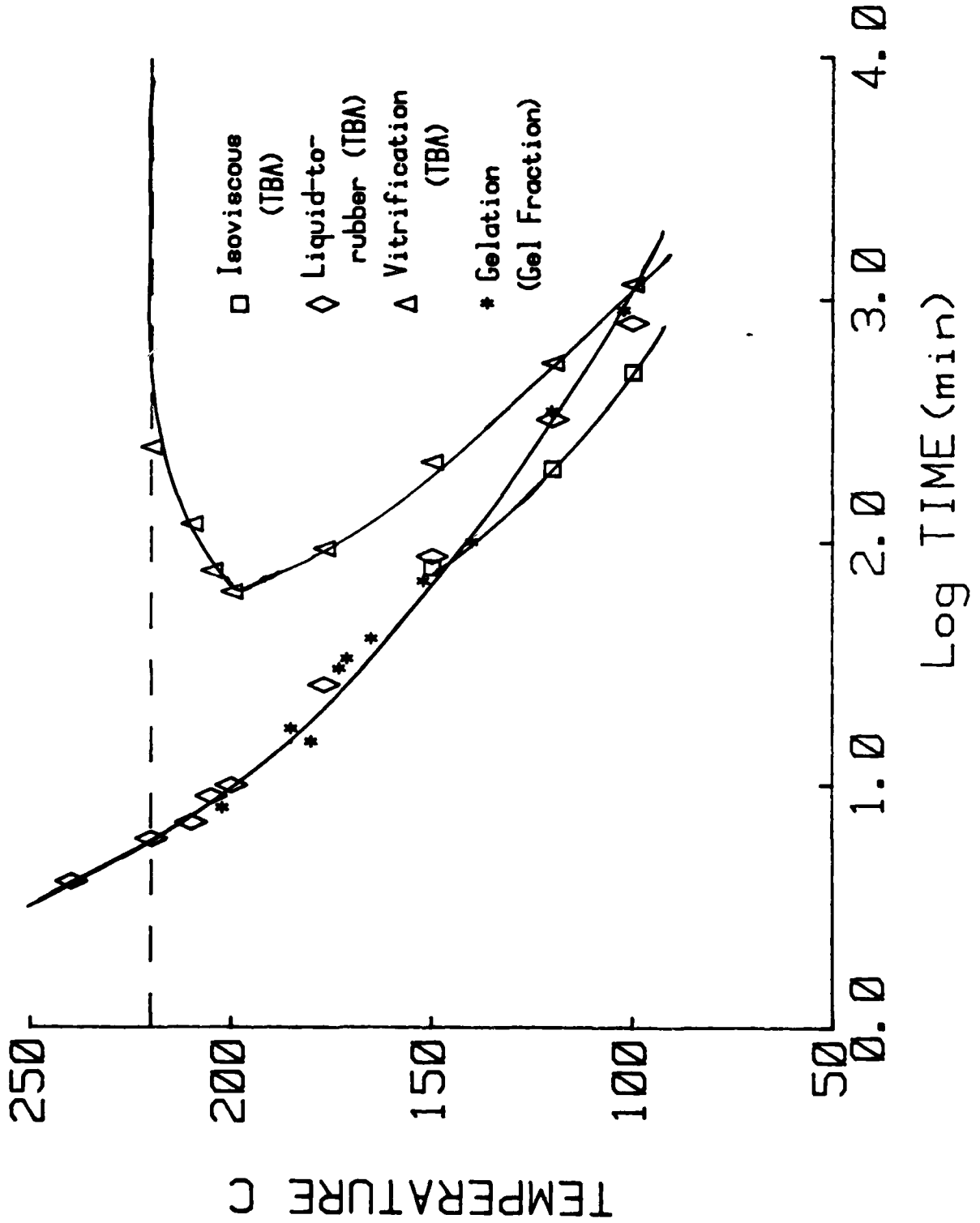


Figure 20

TTT DIAGRAM: EPON 828/DDS

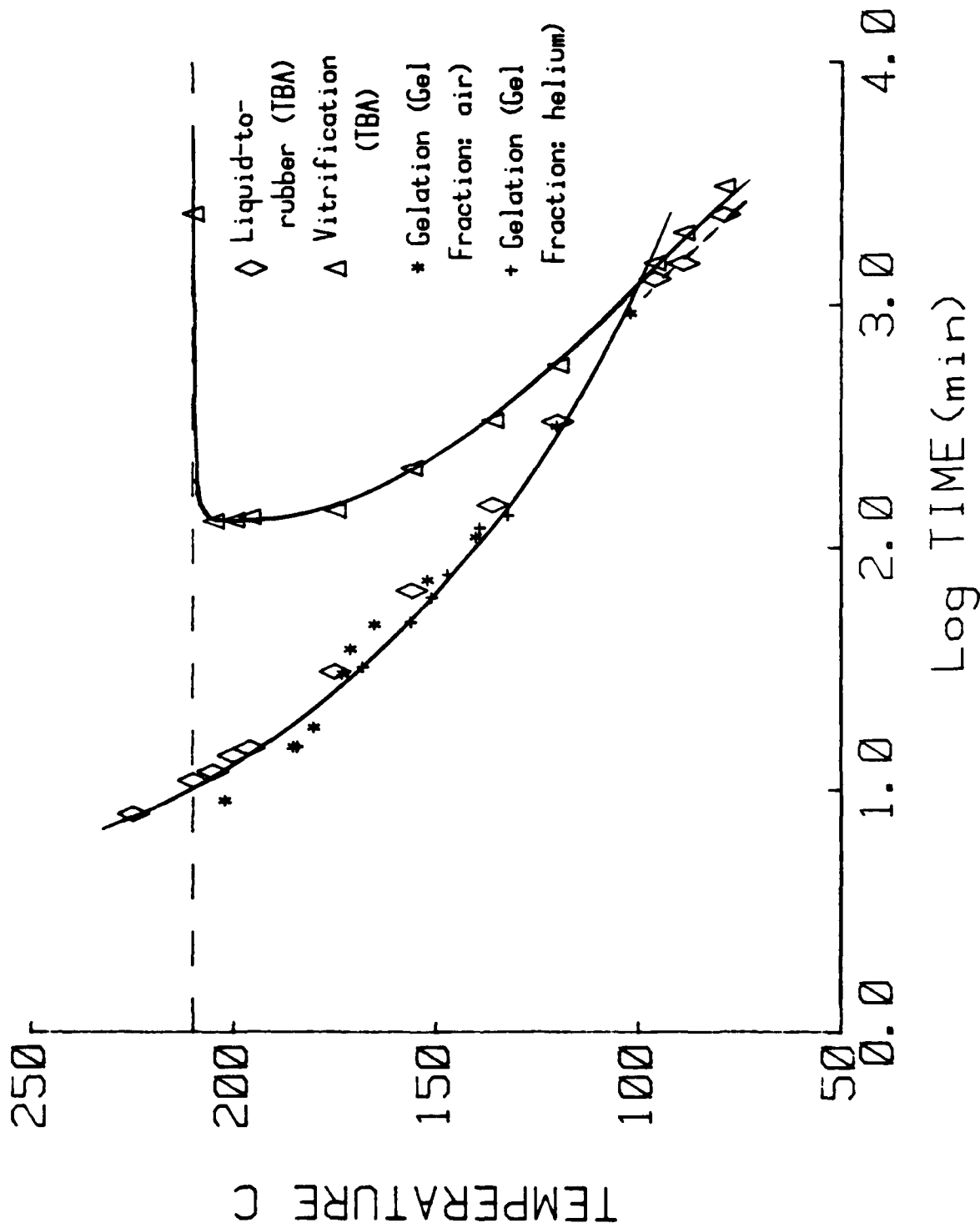


Figure 21

TTT DIAGRAM: EPON 834/DDS

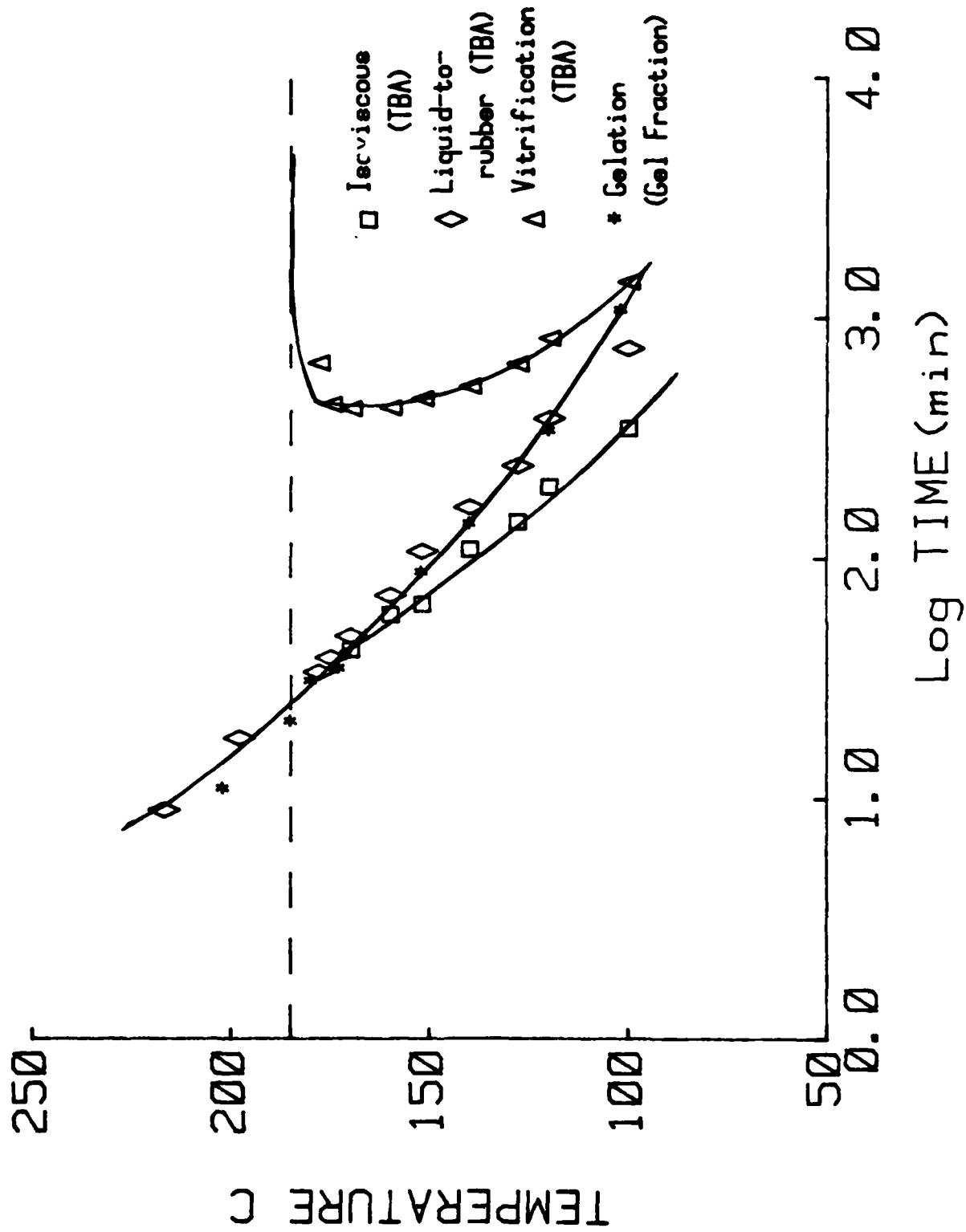


Figure 22

TTT DIAGRAM: EPON 828/MDA

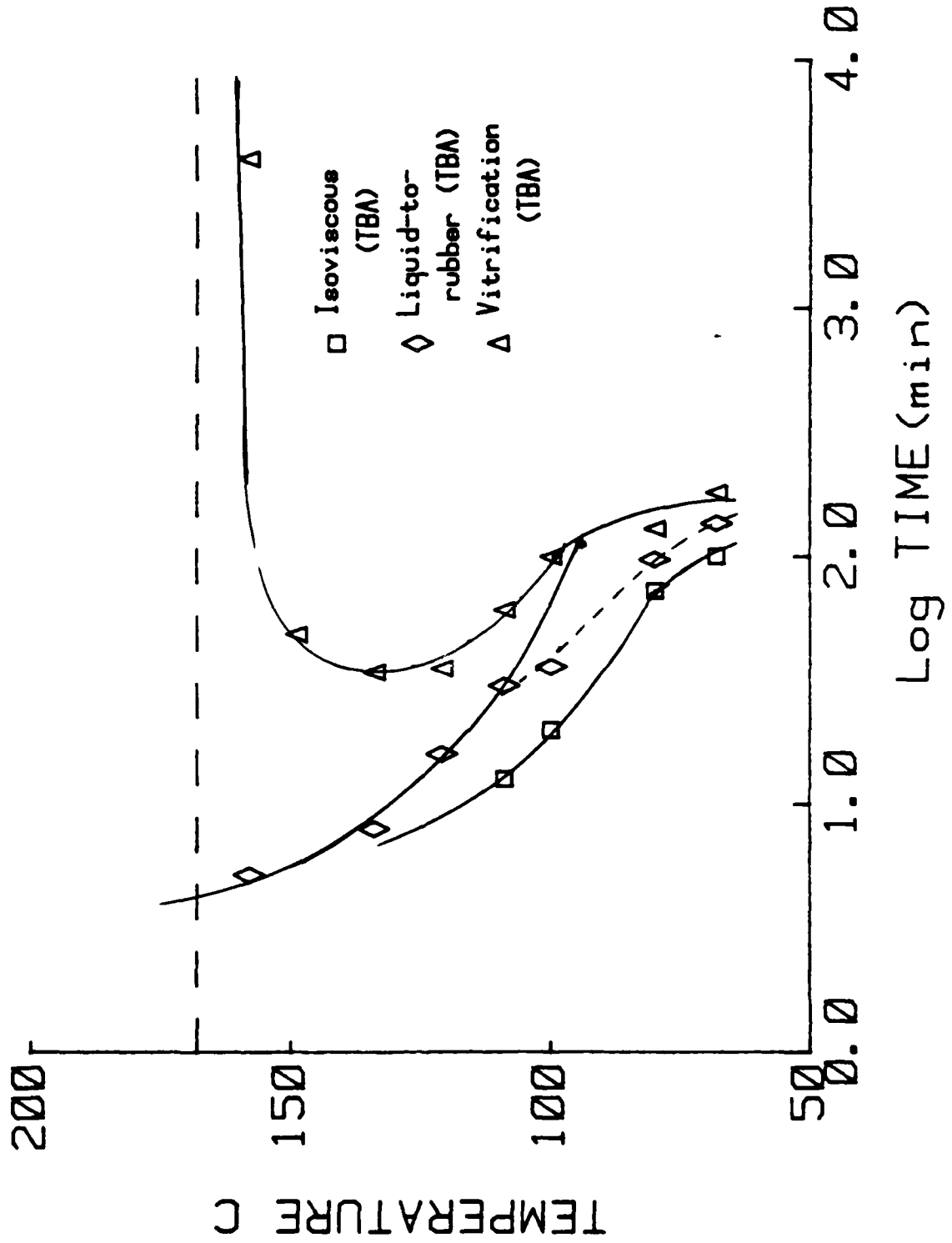


Figure 23

TTT DIAGRAM: EPON 828/PACM-20

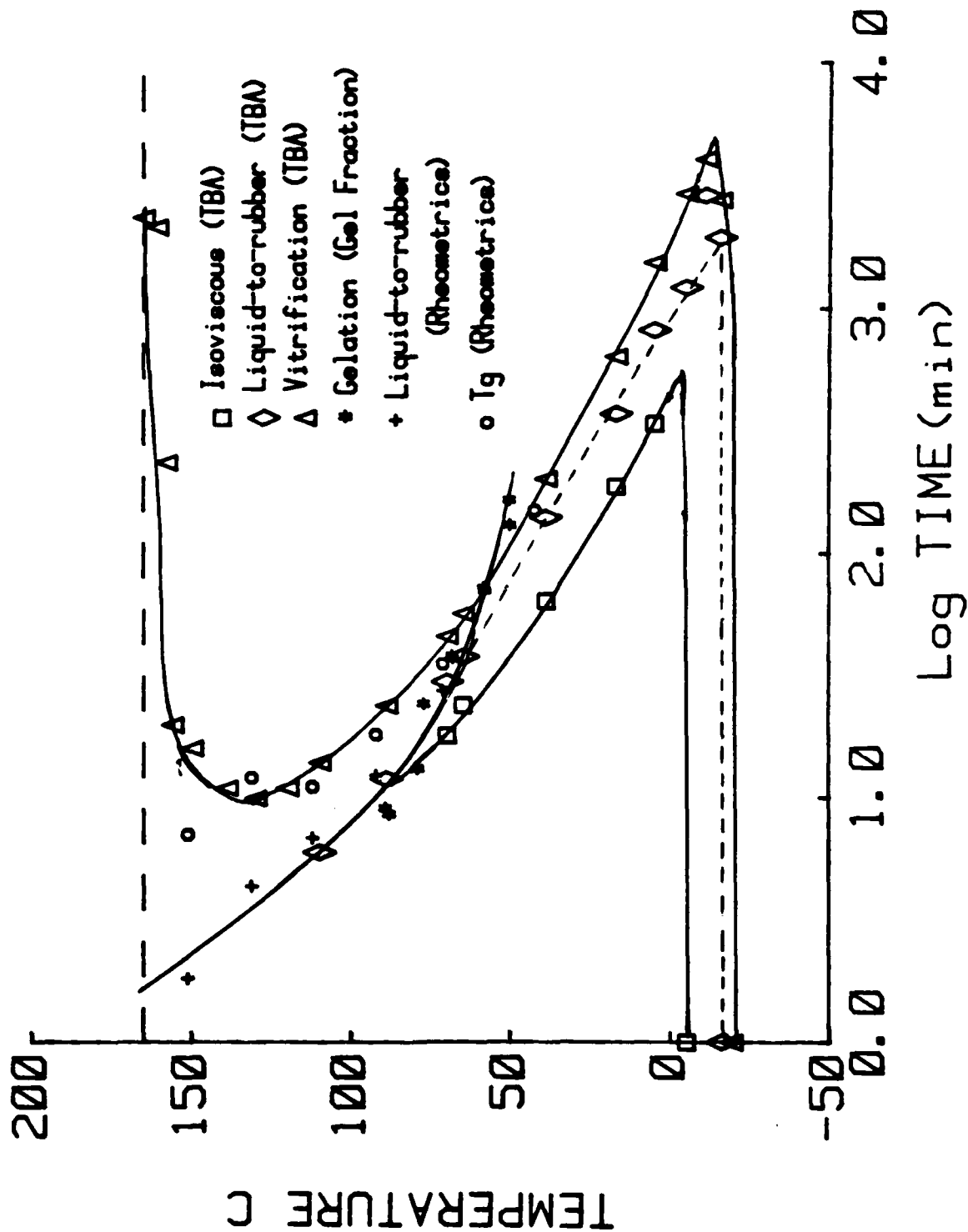


Figure 24

TTT DIAGRAM: EPON 828/TMAB

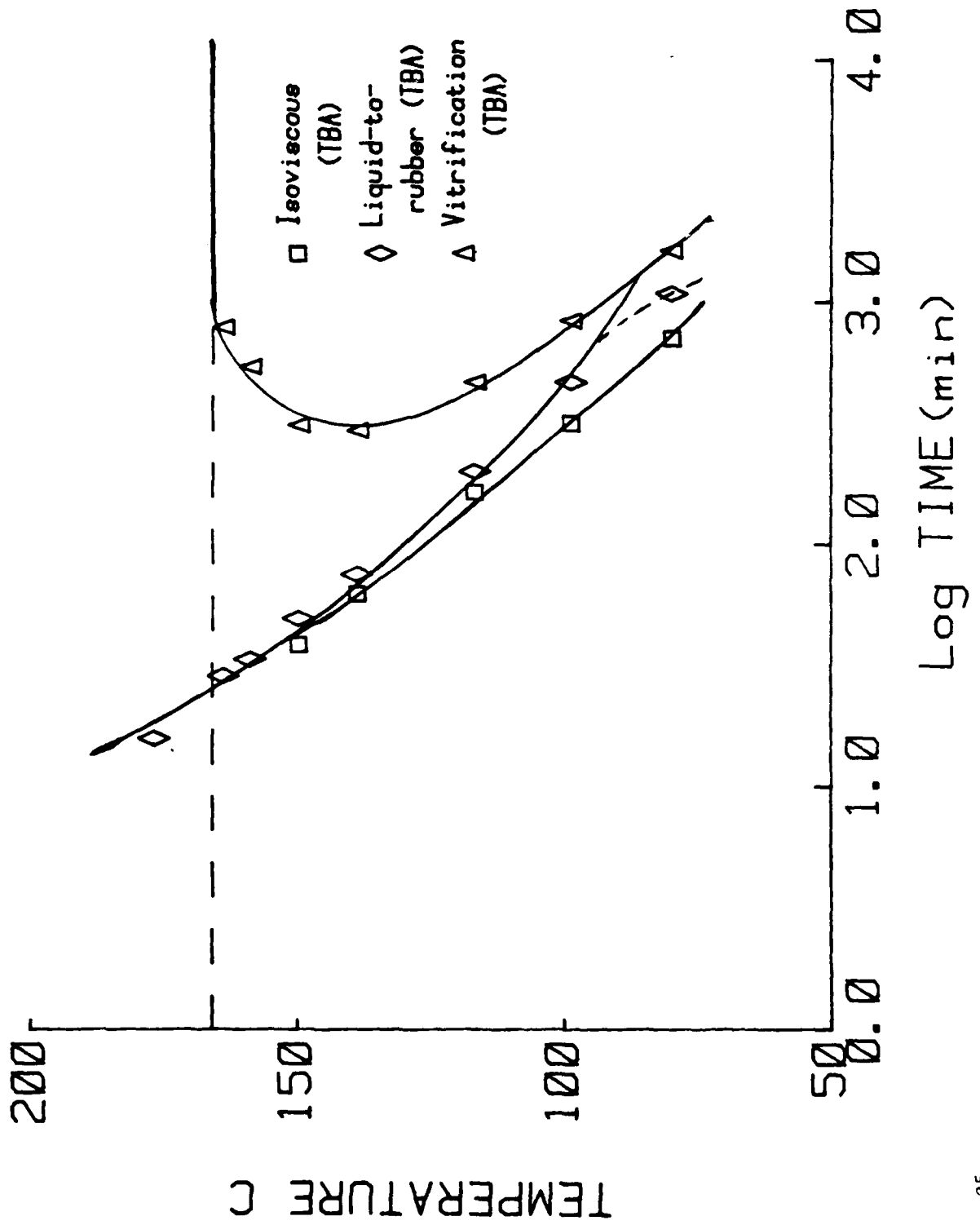


Figure 25

EPON 828/PACM-20

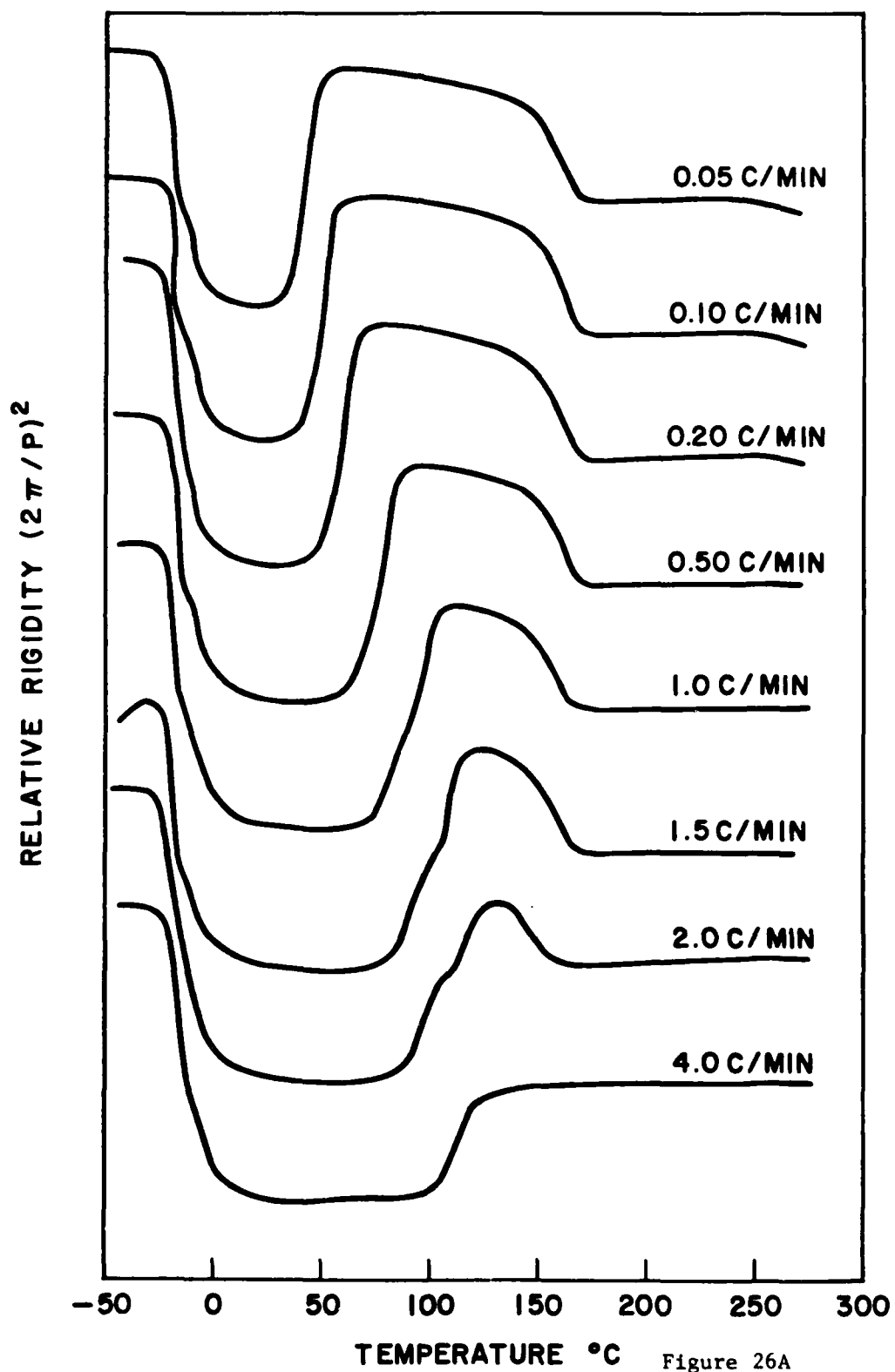


Figure 26A

EPON 828/PACM-20

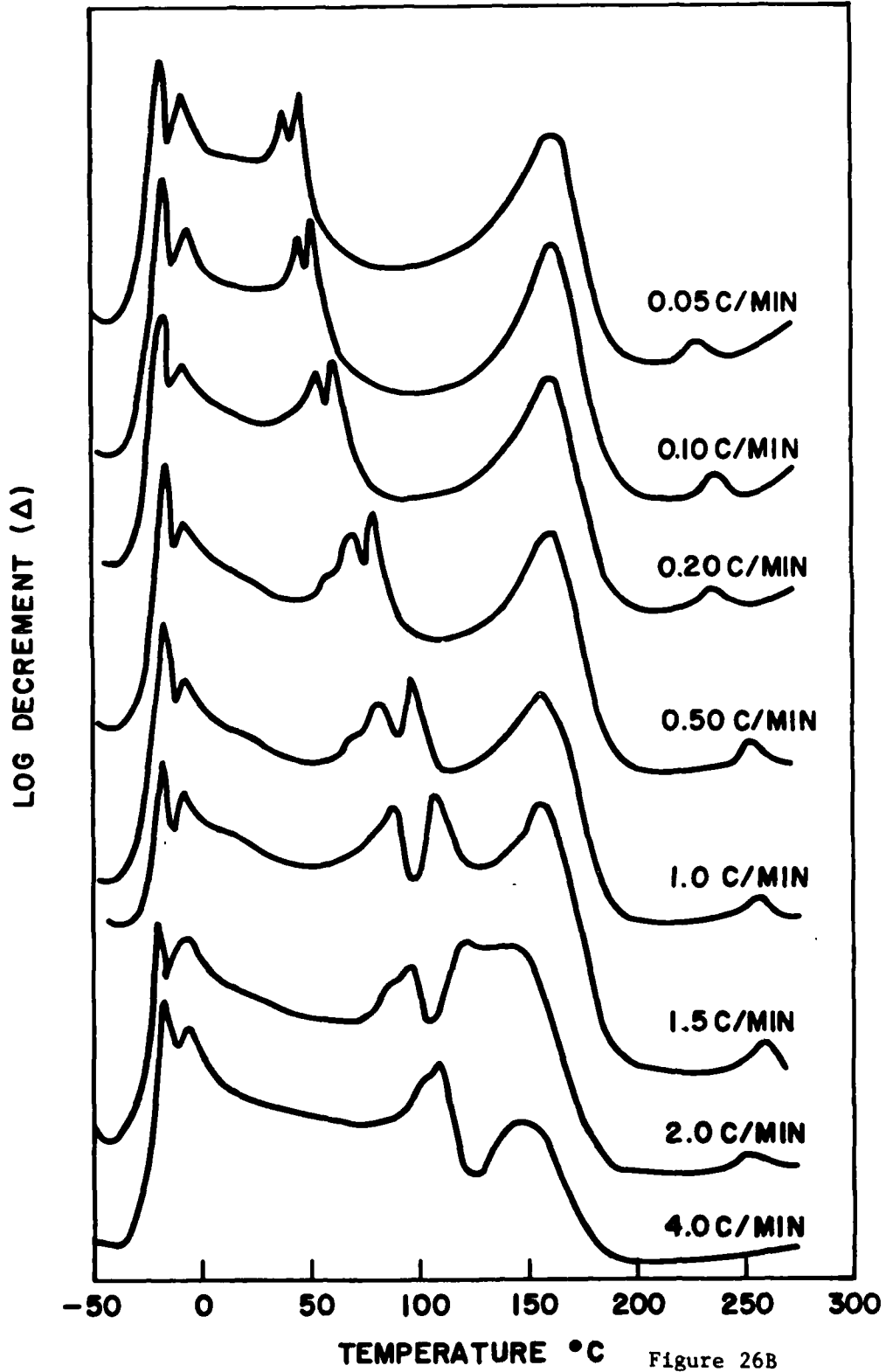


Figure 26B

CHT DIAGRAM: EPON 828/PACM-20

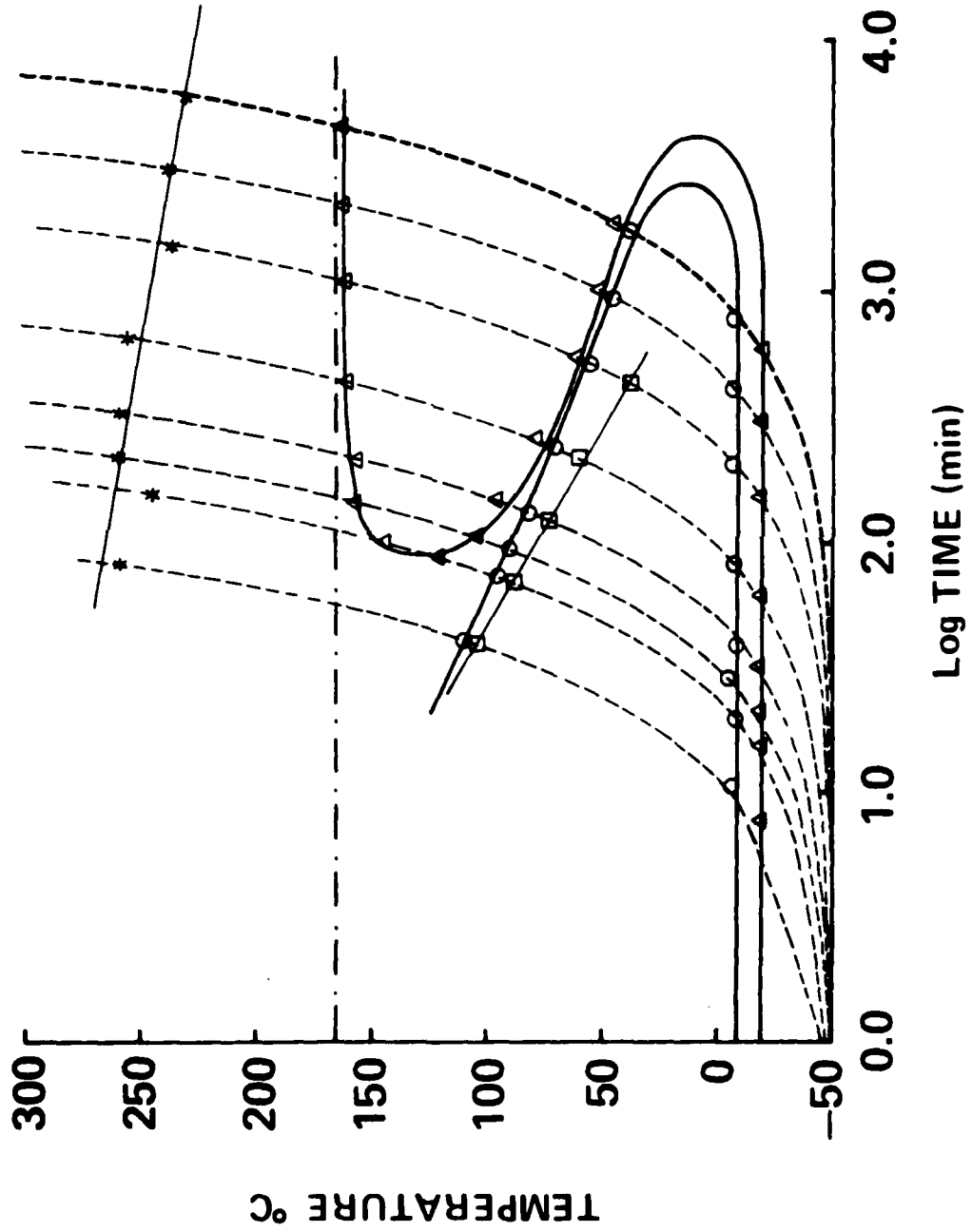


Figure 27

TECHNICAL REPORT DISTRIBUTION LIST, GEN

	<u>No.</u> <u>Copies</u>		<u>No.</u> <u>Copies</u>
Office of Naval Research Attn: Code 413 800 North Quincy Street Arlington, Virginia 22217	2	Naval Ocean Systems Center Attn: Mr. Joe McCartney San Diego, California 92152	1
ONR Pasadena Detachment Attn: Dr. R. J. Marcus 1030 East Green Street Pasadena, California 91106	1	Naval Weapons Center Attn: Dr. A. B. Amster, Chemistry Division China Lake, California 93555	1
Commander, Naval Air Systems Command Attn: Code 310C (H. Rosenwasser) Department of the Navy Washington, D.C. 20360	1	Naval Civil Engineering Laboratory Attn: Dr. R. W. Drisko Port Hueneme, California 93401	1
Defense Technical Information Center Building 5, Cameron Station Alexandria, Virginia 22314	12	Dean William Tolles Naval Postgraduate School Monterey, California 93940	1
Dr. Fred Saalfeld Chemistry Division, Code 6100 Naval Research Laboratory Washington, D.C. 20375	1	Scientific Advisor Commandant of the Marine Corps (Code RD-1) Washington, D.C. 20380	1
U.S. Army Research Office Attn: CRD-AA-IP P. O. Box 12211 Research Triangle Park, N.C. 27709	1	Naval Ship Research and Development Center Attn: Dr. G. Bosmajian, Applied Chemistry Division Annapolis, Maryland 21401	1
Mr. Vincent Schaper DTNSRDC Code 2803 Annapolis, Maryland 21402	1	Mr. John Boyle Materials Branch Naval Ship Engineering Center Philadelphia, Pennsylvania 19112	1
Naval Ocean Systems Center Attn: Dr. S. Yamamoto Marine Sciences Division San Diego, California 91232	1	Mr. A. M. Anzalone Administrative Librarian PLASTEC/ARRADCOM Bldg 3401 Dover, New Jersey 07801	1

TECHNICAL REPORT DISTRIBUTION LIST, 356A

	<u>No. Copies</u>		<u>No. Copies</u>
Dr. M. Broadhurst Bulk Properties Section National Bureau of Standards U. S. Department of Commerce Washington, D.C. 20234	2	Dr. K. D. Pae Department of Mechanics and Materials Science Rutgers University New Brunswick, New Jersey 08903	1
Naval Surface Weapons Center Attn: Dr. J. M. Augl, Dr. B. Hartman White Oak Silver Spring, Maryland 20910	1	NASA-Lewis Research Center Attn: Dr. T. T. Serofini, MS-49-1 2100 Brookpark Road Cleveland, Ohio 44135	1
Dr. G. Goodman Globe Union Incorporated 5757 North Green Bay Avenue Milwaukee, Wisconsin 53201	1	Dr. Charles H. Sherman Code TD 121 Naval Underwater Systems Center New London, Connecticut 06320	1
Professor Hatsuo Ishida Department of Macromolecular Science Case-Western Reserve University Cleveland, Ohio 44106	1	Dr. William Risen Department of Chemistry Brown University Providence, Rhode Island 02191	1
Dr. David Soong Department of Chemical Engineering University of California Berkeley, California 94720		Mr. Robert W. Jones Advanced Projects Manager Hughes Aircraft Company Mail Station D 132 Culver City, California 90230	1
Dr. Curtis W. Frank Department of Chemical Engineering Stanford University Stanford, California 94035		Dr. C. Giori IIT Research Institute 10 West 35 Street Chicago, Illinois 60616	
Picatinny Arsenal Attn: A. M. Anzalone, Building 3401 SMUPA-FR-M-D Dover, New Jersey 07801	1	Dr. R. S. Roe Department of Materials Science and Metallurgical Engineering University of Cincinnati Cincinnati, Ohio 45221	1
Dr. J. K. Gillham Department of Chemistry Princeton University Princeton, New Jersey 08540	1	Dr. Robert E. Cohen Chemical Engineering Department Massachusetts Institute of Technology Cambridge, Massachusetts 02139	1
Dr. E. Baer Department of Macromolecular Science Case Western Reserve University Cleveland, Ohio 44106	1	Dr. T. P. Conlon, Jr., Code 3622 Sandia Laboratories Sandia Corporation Albuquerque, New Mexico	1

TECHNICAL REPORT DISTRIBUTION LIST, 356A

	<u>No.</u> <u>Copies</u>		<u>No.</u> <u>Copies</u>
Dr. Martin Kaufman Code 38506 Naval Weapons Center China Lake, California 93555	1	Professor C. S. Paik Sung Department of Materials Sciences and Engineering Room 8-109 Massachusetts Institute of Technology Cambridge, Massachusetts 02139	1
Professor S. Senturia Department of Electrical Engineering Massachusetts Institute of Technology Cambridge, Massachusetts 02139	1	Professor Brian Newman Department of Mechanics and Materials Science Rutgers, The State University Piscataway, New Jersey 08854	1
Dr. T. J. Reinhart, Jr., Chief Composite and Fibrous Materials Branch Nonmetallic Materials Division Department of the Air Force Air Force Materials Laboratory (AFSC) Wright-Patterson AFB, Ohio 45433	1	Dr. John Lundberg School of Textile Engineering Georgia Institute of Technology Atlanta, Georgia 30332	1
Dr. J. Lando Department of Macromolecular Science Case Western Reserve University Cleveland, Ohio 44106	1		
Dr. J. White Chemical and Metallurgical Engineering University of Tennessee Knoxville, Tennessee 37916	1		
Dr. J. A. Manson Materials Research Center Lehigh University Bethlehem, Pennsylvania 18015	1		
Dr. R. F. Helmreich Contract RD&E Dow Chemical Co. Midland, Michigan 48640	1		
Dr. R. S. Porter Department of Polymer Science and Engineering University of Massachusetts Amherst, Massachusetts 01002	1		
Professor Garth Wilkes Department of Chemical Engineering Virginia Polytechnic Institute and State University Blacksburg, Virginia 24061	1		